

Theory of Impedance Spectroscopy for Lithium Batteries

Fabian Single,^{†,‡} Birger Horstmann,^{*,¶,†,‡} and Arnulf Latz^{*,¶,†,‡}

[†]*German Aerospace Center (DLR), Institute of Engineering Thermodynamics, Pfaffenwaldring 38-40, 70569 Stuttgart, Germany*

[‡]*Helmholtz Institute Ulm (HIU), Helmholtzstraße, 11, 89081 Ulm, Germany*

[¶]*University of Ulm, Albert-Einstein-Allee 47, 89081 Ulm, Germany*

E-mail: birger.horstmann@dlr.de; arnulf.latz@dlr.de

Abstract

In this article, we derive and discuss a physics-based model for impedance spectroscopy of lithium batteries. Our model for electrochemical cells with planar electrodes takes into account the solid-electrolyte interphase (SEI) as porous surface film. We present two improvements over standard impedance models. Firstly, our model is based on a consistent description of lithium transport through electrolyte and SEI. We use well-defined transport parameters, e.g., transference numbers, and consider convection of the center-of-mass. Secondly, we solve our model equations analytically and state the full transport parameter dependence of the impedance signals. Our consistent model results in an analytic expression for the cell impedance including bulk and surface processes. The impedance signals due to concentration polarizations highlight the importance of electrolyte convection in concentrated electrolytes. We simplify our expression for the complex impedance and compare it to common equivalent circuit models. Such simplified models are good approximations in concise parameter ranges. Finally, we compare our model with experiments of lithium metal electrodes and find large transference numbers for lithium ions. This analysis reveals that lithium-ion transport through the SEI has solid electrolyte character.

1 Introduction

Impedance spectroscopy is an essential tool for the characterization of electrochemical devices. This method gives insight into phenomena that are otherwise difficult to access. Its non-destructive nature makes it especially suitable for monitoring delicate surface films such as the solid electrolyte interphase (SEI)¹⁻⁴ in lithium-ion batteries.

Interpretation of impedance measurements requires a modeling approach. Today, equivalent circuit models remain the most prominent model type for this purpose.⁵ However, such models often mask the way some parameters influence the impedance. Physics-

based models include these dependencies at the cost of an increased modeling effort. Numerous comprehensive models exist and describe a diverse amount of electrochemical processes and systems. These include cell level models of standard lithium-ion batteries,^{6,7} Li-sulfur batteries,^{8,9} metal-air batteries,¹⁰⁻¹² and fuel cells.¹³ Other models focus on selected electrochemical processes of interest, such as membranes,¹⁴ interface reactions,^{15,16} electrochemical double layers,^{17,18} and growth of surface layers.^{19,20} Such models accurately capture reactions and transport in the complex geometry and morphology of the corresponding system. They are also used for impedance calculations by taking into account interface capacities.²¹ Then, one can calculate the cell impedance with a single voltage step simulation.²²

Several models discuss the impedance of lithium-ion batteries. Most of these models go to great lengths to describe the porous electrode and the frequency dependent response of single electrode particles. This is described within the framework of 1+1D Newman models.^{23,24} Advanced models consider a particle size distribution²⁵ and anisotropic particles.²⁶ More recent publications also discuss the distribution of relaxation times²⁷ and consider higher harmonics.²⁸

Most of the impedance models cited above are either semi-analytic or fully numeric. However, only exact analytic models allow the use of impedance spectroscopy to determine parameters and physical quantities, e.g., diffusion coefficient, Tafel slope, and double layer capacitance. This is the added value of exact analytic results as demonstrated by Kulikovskiy et al. with multiple impedance models for fuel cells.²⁹⁻³¹

In our impedance model we consider a simple cell geometry with two planar electrodes. This results in exact analytical expressions which elucidate the full parameter dependence of the complex resistance. We give particular attention to the electrolyte which is described with a thermodynamically consistent theory. Our theory describes a concentrated and non-ideal binary electrolyte with convection. We use the Poisson equation which naturally describes charged surface lay-

ers. These layers cause the standard capacitive response in impedance spectroscopy. The Poisson equation is rarely used in literature^{14,32} as most studies simplify the equation system and assume local electroneutrality. They then model interface capacitances phenomenologically.²¹ Our impedance model also takes into account the SEI as a surface film covering the electrode. We assume electrolyte transport in the SEI pores and gain insights into the nature of lithium-ion transport through the SEI by comparing our model with a recent experiment.³³

We briefly summarize our theory based model, and outline our calculation procedure for impedance in sec. 2. These calculations are presented in sec. 3 and discussed in sec. 4. In sec. 5, we validate our impedance model with a comparison to experimental data. Finally, in sec. 6 we give our conclusion.

2 Theory

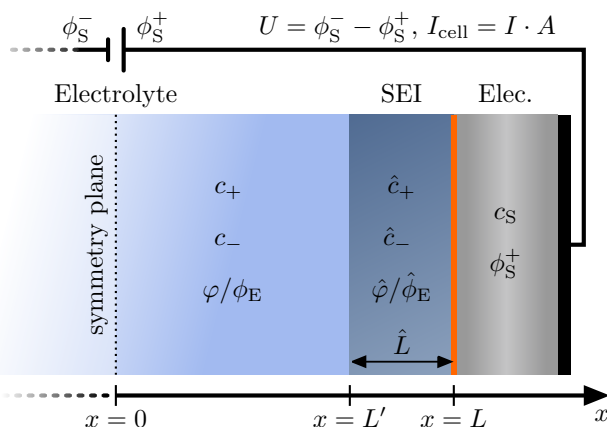


Figure 1: Sketch of the symmetric cell used for the impedance calculation listing relevant variables of each phase. The SEI thickness \hat{L} determines $L' = L - \hat{L}$. The orange boundary between SEI and electrode marks the location of the interface reaction.

We calculate the half-cell impedance of the symmetric cell depicted in fig. 1. It consists of two identical planar electrodes which are separated by the SEI and a binary electrolyte. This setup represents a common electrochemical cell, e.g., two lithium metal electrodes with LP30 electrolyte. We describe liquid phases such as the electrolyte and the pore space of the SEI with and without the assumption of local electroneutrality. Additionally, we consider a simplified model without SEI in each of these scenarios. Thus, we discuss a total of four impedance models. In this way we guide the reader through calculations and discussions as the model complexity increases.

We perform a virtual experiment to calculate the impedance response of our model cells. To this aim, we apply an oscillating potential or current. Specifically, we choose a boundary condition for which the temporal progression of the “applied” quantity is proportional

to $e^{i\omega t}$. Here, i is the imaginary unit and $\omega = 2\pi f$ is a fixed frequency. We then calculate the corresponding response for this frequency, i.e., current or potential. All governing equations are linearized for this calculation such that a real-valued solution can be obtained easily from the complex one. We find the general solution for each primary variable listed in fig. 1. General solutions are a linear superposition of multiple partial solutions because of the linear nature of the problem. The correct linear combination follows from physical boundary conditions. Considering these constraints naturally results in a linear system of equations. Its solution gives the half cell impedance with the conventional definition

$$Z(\omega) = \frac{U}{2I} = \frac{1}{2} \cdot \frac{\phi_S^- - \phi_S^+}{j_I + j_S}, \quad (1)$$

where the sign in the definition of the voltage difference U considers the difference between technical and physical current. j_I is the current density corresponding to the rate of the interface reaction. j_S describes charge that moves between the electrodes to screen charged surface species, see sec. 3.2.1. Equation (1) gives the impedance in Ωm^2 because j_I , j_S , and I are current densities. Division of $Z(\omega)$ by A , the cross section area of the cell, results in the actual cell resistance.

2.1 Transport Theory

We describe transport in the electrolyte phase with a theory derived by Schammer et al.³⁴ based on previous works in refs 35–38. The theory is discussed in the Electronic Supporting Information, see secs. SI-1 and SI-3. It describes the fluxes of a binary electrolyte consisting of cations, anions and neutral solvent molecules (labelled with *subscript* +, −, and N). Two independent flux expressions are sufficient to describe the motion of this mixture relative to the center-of-mass velocity v , e.g.,

$$N_\alpha = - \sum_{\beta=\pm} D_{\alpha\beta} \nabla c_\alpha - \frac{t_\alpha \kappa}{z_\alpha F} \nabla \phi_E, \quad (2)$$

where $\alpha = \pm$. This representation is well suited to describe a general electrolyte. If we assume local electroneutrality, however, we choose the anion flux N_- and the ionic current \mathcal{J} as independent fluxes

$$N_- = -D_{\text{salt}} \nabla c_- + \frac{t_- \mathcal{J}}{z_- F}, \quad (3a)$$

$$\mathcal{J} = \frac{\mathcal{N} t_- \kappa}{z_+ F} \frac{d\tilde{\mu}_{\text{salt}}}{dc_{\text{salt}}} \nabla c_- - \kappa \nabla \tilde{\varphi}, \quad (3b)$$

where F is the Faraday constant and $\mathcal{N} = \frac{n_+ + n_-}{n_+ n_-}$. Note that N_α and \mathcal{J} are flux and current densities. Fluxes in eqs. (2) and (3) are driven by gradients of concentration c_α , electric potential ϕ_E , and effective electrochemical potential $\tilde{\varphi} = \phi_E + \frac{\tilde{\mu}_+}{z_+ F}$. Effective quantities are marked with a tilde and appear frequently in this work. They originate from the description relative to the center-of-

mass velocity. The effective chemical potential of cation $\tilde{\mu}_+$ and salt $\tilde{\mu}_{\text{salt}}$ are directly related to the conventional quantities, see eqs. (SI-4) and (SI-47). Transport in the electrolyte is parametrized by the salt diffusion coefficient D_{salt} , conductivity κ , and the transference number t_+ ($t_+ + t_- = 1$). The diffusion matrix \mathbf{D} with entries $D_{\alpha\beta}$ in eq. (2) is determined by these three parameters, see sec. SI-3 B. Transport parameters are related to the more fundamental Onsager coefficients by the chemical potentials μ_α . We use the standard definition of the chemical potentials,

$$\mu_\alpha = RT \ln \left(\frac{f_\alpha c_\alpha}{c_{\alpha,0}} \right), \quad \alpha = \pm, \text{salt}, \quad (4)$$

where $c_{\alpha,0}$ are the reference concentrations. The activity coefficients f_α describe the non-ideal behaviour of species α and are related to the thermodynamic coefficient $\mathcal{F}_\alpha = 1 + \frac{\partial \ln \mu_\alpha}{\partial \ln c_\alpha}$, see sec. SI-3 A.

The center-of-mass velocity \mathbf{v} is used to express the complete flux expressions

$$\mathbf{N}_\alpha^* = \mathbf{N}_\alpha + c_\alpha \mathbf{v}. \quad (5)$$

Below, the superscript $*$ labels quantities and parameters that are associated with the complete flux expressions. These flux expressions are used in mass balance equations

$$\partial_t c_\alpha = -\nabla \cdot \mathbf{N}_\alpha^*, \quad (6)$$

which determine the temporal evolution of a concentration with the corresponding flux density. As outlined in sec. SI-1 B, we consider incompressibility as an additional constraint to express \mathbf{v} .^{37,39}

2.2 Linearization of Model Equations

Impedance measurements are performed around an equilibrium state, the reference state. They capture the linear response of this system to an applied potential/current which is oscillating at a given frequency. Because the reference shall not be perturbed, the applied voltage/current must be small. In our analytical approach, these oscillations are chosen to have an infinitesimal amplitude. As a result, any deviation from the reference state in our virtual measurement becomes infinitesimal. Therefore, all governing equations can be linearized around the reference state. Considering eqs. (2) and (3), the most simple such reference state has a constant concentration and potential distribution

$$c_\pm(x) = c_{\pm,0} = n_\pm c_{\text{salt},0}, \quad (7a)$$

$$\phi_E(x) = \phi_{E,0}, \text{ etc.} \quad (7b)$$

Henceforth, we mark all quantities referring to the reference state with the subscript 0. We refer the interested reader to sec. SI-2, where the linearization procedure is described in detail. Linearization of the flux expressions

relative to the center-of-mass velocity results in

$$\mathbf{N}_\alpha = - \sum_{\beta=\pm} D_{\alpha\beta} \nabla \delta c_\beta - \frac{t_\alpha \kappa}{z_\alpha F} \nabla \delta \phi_E, \quad (8a)$$

$$\mathbf{N}_- = -D_{\text{salt}} \nabla \delta c_- + \frac{t_- \mathcal{J}}{z_- F}, \quad (8b)$$

$$\mathcal{J} = \frac{\mathcal{N} t_- \kappa}{z_+ F} \frac{d\tilde{\mu}_{\text{salt}}}{dc_{\text{salt}}} \nabla \delta c_- - \kappa \nabla \delta \tilde{\varphi}. \quad (8c)$$

Linearizing the full flux expressions given by eq. (5) results in

$$\mathbf{N}_\alpha^* = - \sum_{\beta=\pm} D_{\alpha\beta}^* \nabla \delta c_\beta - \frac{t_\alpha^* \kappa}{z_\alpha F} \nabla \delta \phi_E + c_\alpha \mathbf{v}_{\text{off}}, \quad (9a)$$

$$\mathbf{N}_-^* = -D_{\text{salt}}^* \nabla \delta c_- + \frac{t_-^* \mathcal{J}}{z_- F} + c_- \mathbf{v}_{\text{off}}, \quad (9b)$$

$$\mathcal{J}^* = \frac{\mathcal{N} t_- \kappa}{z_+ F} \frac{d\tilde{\mu}_{\text{salt}}}{dc_{\text{salt}}} \nabla \delta c_- - \kappa \nabla \delta \tilde{\varphi} = \mathcal{J}, \quad (9c)$$

where, \mathbf{v}_{off} is a constant offset velocity. Note that eq. (9c) is identical to eq. (8c) because the charge density in our reference state is zero. 2 The linearized flux expressions have three significant properties. *Firstly*, all original variables are replaced with the corresponding deviation variables. They consider the deviation from the reference state

$$c_\alpha \rightarrow \delta c_\alpha = c_\alpha - c_{\alpha,0}, \quad (10a)$$

$$\phi_E \rightarrow \delta \phi_E = \phi_E - \phi_{E,0}, \text{ etc.} \quad (10b)$$

Secondly, all quantities beside these deviation variables are constant after linearization. This not only applies to transport parameters but also to the concentrations c_α and partial derivatives such as $\frac{d\tilde{\mu}_{\text{salt}}}{dc_{\text{salt}}}$. These quantities are consistently evaluated at the reference state. We therefore omit the corresponding notation in each linearized expression. *Thirdly*, a new set of apparent transport parameters (D_{salt}^* , $D_{\alpha\beta}^*$, and t_α^*) consistently replaces the original ones in the linearized full flux expressions. These quantities combine diffusion/migration and convection in a single diffusion/migration term. This is a result of linearizing the expression for the center-of-mass velocity. Equation (SI-64) relates the apparent transport parameters to the parameters used in flux expression relative to the center-of-mass velocity.

2.3 Interface Reaction

We use a linearised Butler-Volmer rate expression to describe the interface reaction rate

$$j_I = \frac{\eta_{\text{lin}}}{\mathcal{R}}. \quad (11)$$

Here, \mathcal{R} is the interface resistance parameter of our model. It is inversely proportional to the exchange current density. Note that eq. (11) does not depend on the charge transfer coefficient and the electrolyte/electrode concentration. These dependencies are part of the non-linearized rate expression.⁴⁰⁻⁴² They vanish because the

expression is linearized at the reference state where $\eta = 0$. The linearized overpotential is equal to

$$\eta_{\text{lin}} = \delta\phi_{\text{S}} - \delta\varphi^{\text{bulk}} - \frac{\partial U}{\partial c_{\text{S}}} \delta c_{\text{S}}, \quad (12)$$

see ref. 41. This expression takes into account the electrode potential $\delta\phi_{\text{S}}$, the electrochemical potential in the electrolyte $\delta\varphi^{\text{bulk}}$, and the concentration of intercalated particles in the electrode δc_{S} . The label ‘‘bulk’’ indicates that the evaluation of $\delta\varphi$ is non-trivial in the case of spatially resolved double layers. For simplicity we restrict ourselves to metallic electrodes, i.e., $\frac{\partial U}{\partial c_{\text{S}}} = 0$, in the main text. The impact of an intercalation electrode is discussed in sec. SI-6. In our definition, η is negative for intercalation or plating processes.

2.4 SEI Model

Experimental and theoretical studies report that SEI is at least partially porous.^{3,19,43–45} Our recent findings suggest that solvent molecules are effectively immobilized within these pores.^{46,47} However, this result does not apply to smaller and more mobile lithium ions. They are also charged and subject to large electric forces. We follow this idea in this work and model the SEI with nano-sized pores. These pores are filled with electrolyte and enable charge transport through the surface film. Parameters, quantities and variables in the SEI pores are marked with a hat. We use porous electrode theory to describe transport in this pore space.^{6,48–50} This means that we employ the same flux expressions that are used for the electrolyte phase, see eq. (8). However, the original bulk transport parameters are replaced with effective ones

$$\hat{D}_{\text{salt}} = \frac{\varepsilon}{\tau} D_{\text{salt}}, \quad (13a)$$

$$\hat{\kappa} = \frac{\varepsilon}{\tau} \kappa. \quad (13b)$$

Parameters ε and τ (porosity and tortuosity) capture the morphology of the SEI. They are constant in space and time. Additionally, we introduce \hat{t}_+ , a dedicated cation transference number for the SEI phase. This is motivated by findings of Popovic et al.⁵¹ They show that the lithium transference number of a liquid electrolyte can be increased and become close to one if the anion species is immobilized in a mesoporous structure.

2.5 Boundary Conditions

The binary electrolyte is in contact with the electrodes which take up lithium ions only. Therefore, the anion flux density N_-^* vanishes at the electrode interface. At the same time, N_+^* is equal to the interface reaction rate $\frac{j_{\text{I}}}{z_+ F}$. For the electrodes at $x = L$, we obtain the following boundary conditions for the fluxes relative to

the center-of-mass velocity

$$N_{\alpha}(L) = -\frac{j_{\text{I}}}{z_+ F} \cdot \begin{cases} 1 - \frac{\rho_+}{\rho} & \alpha = +, \\ -\frac{z_+ \rho_+}{z_- \rho} & \alpha = -. \end{cases} \quad (14)$$

Here, ρ_+ and ρ are the cation mass density and the mass density of the electrolyte. Sections SI-1 B and SI-3 D contain a detailed derivation of the expression above.

3 Theory of Impedance Spectroscopy

The most common simplification in the modeling of electrochemical systems is the assumption of local electroneutrality. We use this assumption for impedance calculations in sec. 3.1 (neutral models). These calculations are then repeated without the electroneutrality assumption in sec. 3.2 (non-neutral models). We discuss all impedance results in sec. 4.

3.1 Electroneutral Impedance

Local electroneutrality means that the charge density ϱ is zero and that the ionic current \mathcal{J} is constant in space. This assumption also implies that charge does not accumulate at interfaces, therefore the double layer screening charge Q_{S} and the corresponding current j_{S} vanish. In this case, we apply an oscillating cell current $I(t) = I_0 e^{i\omega t}$. This is convenient because electroneutrality implies $\mathcal{J} = I$ such that eqs. (8c) and (9b) can be used to solve for δc_- and $\delta\varphi$.

We first calculate the impedance without considering SEI. Thus, the electrolyte phase spans from $-L$ to L and is in direct contact with the electrode. We add SEI in sec. 3.1.3.

In the first step we insert the linearized flux expression for N_-^* into the mass balance equation of the anion concentration eq. (6). This results in a linear partial differential equation in δc_- ,

$$\partial_t \delta c_- = D_{\text{salt}}^* \Delta \delta c_-, \quad (15)$$

as $\nabla \cdot \mathcal{J} = 0$. We solve it with an exponential Ansatz in x and t , i.e. $\delta c_- \propto e^{ikx} e^{i\omega t}$. Only anti-symmetric solutions in x contribute to the impedance calculation, see eq. (1). The solution of eq. (15) then becomes

$$\delta c_- = C e^{i\omega t} \sin(kx), \quad (16)$$

where C is a coefficient and the wave number k is given by the dispersion relation,

$$k = (1 - i) \sqrt{\frac{\omega}{2D_{\text{salt}}^*}}. \quad (17)$$

The inverse of k describes the spatial width of salt concentration oscillations at a given frequency ω . We determine C with the flux boundary condition for the anion

species, see eq. (14),

$$C e^{i\omega t} = \frac{I_0 e^{i\omega t}}{z_- F} \frac{\rho}{\tilde{\rho}_N} \frac{1}{D_{\text{salt}}^*} \left(t_- - \frac{\rho_+}{\rho} \right) \frac{1}{k \cos(kL)}. \quad (18)$$

The extrapolated density $\tilde{\rho}_N$ is given by $\tilde{\rho}_\alpha = \frac{M_\alpha}{\nu_\alpha}$ (M_α is the molar weight and ν_α is the partial molar volume of species α). We find that C is proportional to the amplitude of the applied current I_0 .

Next, we calculate the deviation of the electrochemical potential $\delta\varphi$ at $x = L$. This quantity is needed to express the rate of the interface reaction with eq. (12). We obtain it by integrating eq. (9c). However, first, we express the effective electrochemical potential $\tilde{\varphi}$ in this equation with φ , the conventional one. Equations (SI-4b) and (SI-61) relate these quantities,

$$\tilde{\varphi} = \varphi - \frac{M_+}{M_N} \frac{\mu_N}{z_+ F}. \quad (19)$$

We eliminate the chemical potential of the solvent μ_N with the Gibbs-Duhem relation, see eq. (SI-46). The differential version of eq. (19) then becomes

$$\frac{\partial \delta \tilde{\varphi}}{\partial x} = \frac{\partial \delta \varphi}{\partial x} + \frac{\mathcal{N}}{z_+ F} \frac{\rho_+}{\rho} \frac{d\tilde{\mu}_{\text{salt}}}{dc_{\text{salt}}} \frac{\partial \delta c_-}{\partial x}, \quad (20)$$

where, electrolyte density ρ and cation density ρ_+ are constant and evaluated at the reference state. We use eq. (20) in eq. (9c) and rearrange for $\nabla\varphi$. Integration from 0 to x results in

$$\delta\varphi = -\frac{Ix}{\kappa} + \frac{\mathcal{N}}{z_+ F} \left(t_- - \frac{\rho_+}{\rho} \right) \frac{d\tilde{\mu}_{\text{salt}}}{dc_{\text{salt}}} \cdot \delta c_-(x). \quad (21)$$

The anti-symmetry of concentration and electrochemical potential implies that both δc_- and $\delta\varphi$ vanish at $x = 0$.

3.1.1 Interface Reaction

We describe the interface reaction rate j_I with the linearized Butler-Volmer expression given by eq. (11). In the electroneutral model, we evaluate the electrochemical potential at the interface $\delta\varphi^{\text{bulk}} = \delta\varphi(L)$. The current between the electrodes I and the interface reaction rate j_I are related by

$$I = -j_I = -\eta_{\text{lin}} \mathcal{R}^{-1}, \quad (22)$$

where the sign considers the orientation of the interface. Inserting the linearized overpotential η_{lin} from eq. (12) gives the potential of the electrode

$$\delta\phi_S^\pm = \delta\phi_S(+L) = -IR + \delta\varphi(L). \quad (23)$$

3.1.2 Impedance

Considering the symmetry of the solution implies $U = \phi_E^- - \phi_E^+ = -2\delta\phi_E^+$. Equation (1) then implies $Z = \delta\phi_S^+/I$ if $j_S = 0$ is considered. Therefore, we obtain the complex impedance by inserting eq. (21) in eq. (23),

considering eqs. (16) and (18), and dividing by I . We find that Z is the sum of three distinct contributions

$$Z(\omega) = R_E + R_I + R_D \cdot \underbrace{\frac{\tan(kL)}{kL}}_{Z_D}. \quad (24)$$

The complex impedance depends on frequency ω through the dispersion relation $k(\omega)$, see eq. (17). Here, the ohmic contributions R_E , R_I and R_D are constant and do not depend on frequency,

$$R_E = \frac{L}{\kappa}, \quad (25a)$$

$$R_I = \mathcal{R}, \quad (25b)$$

$$R_D = \frac{-\mathcal{N}}{z_+ z_- F^2} \frac{L}{D_{\text{salt}}^*} \left(t_- - \frac{\rho_+}{\rho} \right)^2 \frac{\rho^2}{\underbrace{\rho_N \tilde{\rho}_N}_{\mathcal{M}}} \frac{d\mu_{\text{salt}}}{dc_{\text{salt}}}. \quad (25c)$$

We attribute R_E and R_I to the resistance of the electrolyte and the interface reaction. R_D and Z_D describe a finite-length Warburg impedance or Warburg Short (W_S).^{52,53} This is the impedance increase of the electrolyte as salt concentration gradients form at low frequencies. The cation density $\rho_+ = M_+ c_+$ and solvent density $\rho_N = M_N c_N$ as well as $\tilde{\rho}_N = M_N \nu_N^{-1}$ determine R_D in eq. (25c). The relative cation density ρ_+/ρ appears as a correction of the transference number t_- . It vanishes in the dilute limit. We rewrite the factor \mathcal{M} as a function of $\alpha = c_{\text{salt}} \nu_{\text{salt}}$ and $\beta = \tilde{\rho}_{\text{salt}}/\tilde{\rho}_N$ ($\tilde{\rho}_{\text{salt}} = M_{\text{salt}}/\nu_{\text{salt}}$)

$$\mathcal{M} = \frac{\rho^2}{\rho_N \tilde{\rho}_N} = (1 - \alpha) \left(1 + \frac{\alpha\beta}{1 - \alpha} \right)^2. \quad (26)$$

This factor has a non-linear dependence on the salt concentration through α . It approaches one in the dilute limit and diverges at the maximum salt concentration ν_{salt}^{-1} .

3.1.3 Solid-Electrolyte Interphase

The SEI covers negative electrodes in Li-ion batteries. In this subsection, we take SEI into account as a porous surface film, see sec. 2.4 and fig. 1. As described in sec. 2, we use porous electrode theory to describe transport in this interphase.^{6,48-50} To this aim, we replace the transport parameters in eqs. (9b) and (9c) with effective parameters for the SEI phase. We use these expressions in the modified mass balance equation, eq. (6), and consider SEI porosity

$$\partial_t(\varepsilon \delta \hat{c}_-) = \hat{D}_{\text{salt}}^* \Delta(\varepsilon \delta \hat{c}_-). \quad (27)$$

This equation describes the temporal evolution of the anion concentration in the SEI pores. In analogy to eq. (16), an exponential Ansatz results in the dispersion

relation

$$\hat{k} = (1 - i) \sqrt{\frac{\tau\omega}{2D_{\text{salt}}^*}} = (1 - i) \sqrt{\frac{\varepsilon\omega}{2\hat{D}_{\text{salt}}^*}}. \quad (28)$$

Here, the symmetry does not simplify the solution. Thus, the anion concentration in the SEI pores contains leftmoving and rightmoving waves

$$\delta\hat{c}_- = e^{i\omega t} \left(\hat{C}^+ e^{i\hat{k}x} + \hat{C}^- e^{-i\hat{k}x} \right). \quad (29)$$

The concentration in the electrolyte phase is given by eq. (16), also in this case. We now determine the three coefficients C , \hat{C}^+ , and \hat{C}^- with interface boundary conditions. Electrolyte and SEI phase share the interface at $x = \pm L'$. Both phases must have the same salt concentration at this point, i.e., $\delta c_-(L') = \delta\hat{c}_-(L')$. The anion flux must also be continuous, i.e., $N_-^*(L') = \hat{N}_-^*(L')$. As the convective flux is identical in both phases we can use $N_-(L') = \hat{N}_-(L')$ instead. The anion flux must satisfy the boundary condition at the electrode interface, see eq. (14). We combine these three constraints in a linear system of equations

$$\begin{pmatrix} \sin(kL') & e^{i\hat{k}L'} & e^{-i\hat{k}L'} \\ k \cos(kL') & -i\hat{k}\frac{\varepsilon}{\tau}e^{i\hat{k}L'} & i\hat{k}\frac{\varepsilon}{\tau}e^{-i\hat{k}L'} \\ 0 & i\hat{k}\frac{\varepsilon}{\tau}e^{i\hat{k}L} & -i\hat{k}\frac{\varepsilon}{\tau}e^{-i\hat{k}L} \end{pmatrix} \vec{C} = \frac{Ie^{-i\omega t}}{z_-FD_{\text{salt}}} \begin{pmatrix} 0 \\ t_- - \hat{t}_- \\ \hat{t}_- - \frac{\rho_{\pm}}{\rho} \end{pmatrix}, \quad (30)$$

where $\vec{C} = (C, \hat{C}^+, \hat{C}^-)^T$ is the coefficient vector. These equations are solved analytically, see eq. (SI-66).

Next, we calculate $\varphi(L)$, the electrochemical potential at the electrode interface. In analogy to eq. (21), we rearrange eq. (8c) and find $\delta\varphi$ by integration and by considering eq. (20)

$$\delta\varphi(L) = -\frac{I}{\kappa} \left(L' + \frac{\tau}{\varepsilon} \hat{L} \right) + \frac{\mathcal{N}}{z_+F} \frac{d\tilde{\mu}_{\text{salt}}}{dc_{\text{salt}}} \left[(t_- - \hat{t}_-) \delta\hat{c}_-(L') + \left(\hat{t}_- - \frac{\rho_{\pm}}{\rho} \right) \delta\hat{c}_-(L) \right]. \quad (31)$$

We integrate over the electrolyte and the porous SEI phase which have different transference numbers t_- and \hat{t}_- . The concentration deviations $\delta\hat{c}_-$ at $x = L'$ and $x = L$ are given by eq. (29) and the solution of eq. (30). Next, we insert $\delta\varphi(L)$ in eq. (23) to express the electrode potential $\delta\phi_{\text{S}}^+$. As in sec. 3.1.2, the half-cell impedance Z is given by $\delta\phi_{\text{S}}^+/I$,

$$Z(\omega) = R'_{\text{E}} + R_{\text{SEI}} + R_{\text{I}} + Z_{\text{D,SEI}} + Z'_{\text{D}}, \quad (32)$$

where $R'_{\text{E}} = L'/\kappa$ is the adjusted resistance of the electrolyte and $R_{\text{SEI}} = \hat{L}/\hat{\kappa}$ is the resistance of the SEI. Here, quantities labeled with ' replace the corresponding quantities in the model without SEI eq. (24). The interface resistance R_{I} is still given by eq. (25b). $Z_{\text{D,SEI}}$ and

Z'_{D} are stated in eq. (33). They describe the impedance increase due to the build-up of salt concentration profiles in SEI and electrolyte phase. The length and diffusion coefficient of each phase (L' , \hat{L} and D_{salt}^* , \hat{D}_{salt}^*) determine a characteristic frequency for this process in each domain.

$$Z'_{\text{D}} = \frac{L'\Theta}{D_{\text{salt}}^*} \left(2(\hat{t}_- - t_-) \left(\hat{t}_- - \frac{\rho_{\pm}}{\rho} \right) \sec(\hat{k}\hat{L}) + (\hat{t}_- - t_-)^2 + \left(\hat{t}_- - \frac{\rho_{\pm}}{\rho} \right)^2 \right) \cdot \frac{\tan(kL')}{\Psi \cdot kL'} \quad (33a)$$

$$Z_{\text{D,SEI}} = \frac{\hat{L}\Theta}{\hat{D}_{\text{salt}}^*} \left(\hat{t}_- - \frac{\rho_{\pm}}{\rho} \right)^2 \cdot \frac{\tan(\hat{k}\hat{L})}{\Psi \cdot \hat{k}\hat{L}}, \quad (33b)$$

where

$$\Theta = \frac{-\mathcal{N}}{z_+z_-F^2} \frac{\rho^2}{\rho_{\text{N}}\tilde{\rho}_{\text{N}}} \frac{d\mu_{\text{salt}}}{dc_{\text{salt}}}, \quad (34a)$$

$$\Psi = 1 - \varepsilon\sqrt{\tau^{-1}} \tan(kL') \tan(\hat{k}\hat{L}). \quad (34b)$$

3.2 General Impedance

In this section, we calculate the impedance without the assumption of local electroneutrality. Without electroneutrality, the number of independent concentrations in the electrolyte increases by one (c_+ and c_-). We use the Poisson equation to account for this new variable

$$-\frac{\varrho}{\varepsilon_0\varepsilon_{\text{R}}} = \Delta\phi_{\text{E}} = \Delta\delta\phi_{\text{E}}. \quad (35)$$

It relates the electrostatic potential in the electrolyte ϕ_{E} with the ionic charge density ϱ . The direct appearance of ϕ_{E} in one of the primary equations makes it reasonable to use ϕ_{E} as a variable instead of the electrochemical potential φ . As a consequence, we use a different set of flux expressions for the non-neutral system (eq. (9a) instead of eqs. (9b) and (9c)). Inserting eq. (9a) into a mass-balance equation for c_+ and c_- results in

$$\partial_t\delta c_{\alpha} = \sum_{\beta=\pm} D_{\alpha\beta}^* \Delta\delta c_{\beta} + \frac{t_{\alpha}^* \kappa}{z_{\alpha} F} \Delta\delta\phi_{\text{E}}. \quad (36)$$

because v_{off} is constant. Now, we use the Poisson equation to eliminate the electric field

$$\partial_t\delta c_{\alpha} = \sum_{\beta=\pm} \left(D_{\alpha\beta}^* \Delta\delta c_{\beta} - \frac{t_{\alpha}^* \kappa}{\varepsilon_0\varepsilon_{\text{R}}} \frac{z_{\beta}}{z_{\alpha}} \delta c_{\beta} \right). \quad (37)$$

Using the vector $\vec{\delta c} = (\delta c_+, \delta c_-)^T$ and the matrix

$$\mathcal{T}^* = \frac{\kappa}{\varepsilon_0\varepsilon_{\text{R}}} \begin{pmatrix} t_+^* & -n_+ n_+^{-1} t_+^* \\ -n_- n_+^{-1} t_-^* & t_-^* \end{pmatrix}, \quad (38)$$

we write eq. (37) in matrix form

$$\partial_t\vec{\delta c} = \mathbf{D}^* \Delta\vec{\delta c} - \mathcal{T}^* \vec{\delta c}, \quad (39)$$

where differential operators are applied element wise. Equation (39) is a coupled linear ODE in $\vec{\delta c}$. We solve this equation with an exponential ansatz

$$\vec{\delta c} = \vec{\eta} \cdot e^{i\omega t} e^{ikx}. \quad (40)$$

$\vec{\eta}$ is a coefficient vector and ω is a fixed frequency. This results in an algebraic matrix equation

$$0 = \left(k^2 \mathcal{I} + \underbrace{\mathbf{D}^{*-1} (\mathcal{T}^* + i\omega \mathcal{I})}_{\mathcal{A}} \right) \vec{\eta}, \quad (41)$$

where \mathcal{I} is the identity matrix. If $\vec{\eta}$ is an eigenvector of \mathcal{A} with eigentwert λ , we obtain

$$k^2 = -\lambda. \quad (42)$$

The matrix \mathcal{A} has two eigenvectors $\vec{\eta}_1$ and $\vec{\eta}_2$ with eigenvalues λ_1 and λ_2 . Note that these eigenvalues and eigenvectors depend on the frequency ω . Below, we scale the eigenvectors of \mathcal{A} so that their second entry equals 1, i.e., $\vec{\eta}_\alpha = (\eta_\alpha, 1)^T$. We then obtain four possible solutions for k

$$k_\alpha^\pm = \pm \sqrt{-\lambda_\alpha}, \quad \alpha = 1, 2. \quad (43)$$

Due to the superposition principle, we obtain the general solution for the concentration deviation

$$\vec{\delta c} = e^{i\omega t} \sum_{\alpha=1,2} \vec{\eta}_\alpha \Gamma_\alpha. \quad (44)$$

The solution is determined by four coefficients C_α^\pm which are contained in the function $\Gamma_\alpha(x)$

$$\Gamma_\alpha(x) = \Gamma_\alpha = C_\alpha^+ e^{ik_\alpha x} + C_\alpha^- e^{-ik_\alpha x}, \quad (45a)$$

$$\Gamma'_\alpha(x) = \Gamma'_\alpha = C_\alpha^+ e^{ik_\alpha x} - C_\alpha^- e^{-ik_\alpha x}, \quad (45b)$$

where $\alpha = 1, 2$. These functions are introduced for readability.

The electrostatic potential ϕ_E in the electrolyte is differentially directly linked to the free charge density via the Poisson equation. We use the concentrations δc_+ and δc_- given by eq. (44) to express $\varrho = F \sum_\alpha z_\alpha \delta c_\alpha$. We then insert it in the Poisson equation and obtain

$$\delta \phi_E = e^{i\omega t} F \left(\sum_{\alpha=1,2} \Pi_\alpha \Gamma_\alpha + \Phi' x + \Phi \right), \quad (46)$$

by integrating twice. Here, Φ' and Φ are integration constants and Π_α is

$$\Pi_\alpha = \frac{z_+ \eta_\alpha + z_-}{\varepsilon_0 \varepsilon_R k_\alpha^2}, \quad \alpha = 1, 2. \quad (47)$$

Six coefficients C_1^\pm , C_2^\pm , Φ' , and Φ define the general solution of $\vec{\delta c}$ and $\delta \phi_E$ for a given frequency ω . We determine these constants with physical boundary conditions in secs. 3.2.5 and 3.2.6. To this aim, the expressions for $\vec{\delta c}$ and $\delta \phi_E$ from eqs. (44) and (46) are inserted

into the flux expression eq. (8a). We then obtain the linearized flux expression relative to the center-of-mass velocity

$$N_\alpha = -e^{i\omega t} \left(\sum_{\beta=1,2} \Omega_{\alpha\beta} \Gamma'_\beta + \frac{t_\alpha \kappa}{z_\alpha} \Phi' \right), \quad (48)$$

where the 2x2 matrix Ω with indices $\alpha = \pm$ and $\beta = 1, 2$ is given by

$$\Omega_{\alpha\beta} = ik_\beta \left(\frac{\kappa t_\alpha}{z_\alpha} \Pi_\beta + D_{\alpha+} \eta_\beta + D_{\alpha-} \right). \quad (49)$$

3.2.1 Double Layer Screening Current

Usually, solid electrodes are electronically highly conductive. We assume that this conductivity is infinite which is a good approximation for metal electrodes or graphite. Thus, the potential within the electrode is spatially constant, see fig. 3. Therefore, the electric potential has a kink at the interface between the electrode and the electrolyte. This implies charge accumulation at the interface according to Gauss' law. This charge is provided by free charge carriers (electrons) from the electrode. It is determined by the potential gradient in the electrolyte at the interface

$$Q_S = \varepsilon_0 \varepsilon_R \left. \frac{\partial \phi_E}{\partial x} \right|_{x=L} = \varepsilon_0 \varepsilon_R \left. \frac{\partial \delta \phi_E}{\partial x} \right|_{x=L}. \quad (50)$$

The current which supplies these charges is obtained from the temporal derivative of Q_S

$$j_S = \frac{\partial Q_S}{\partial t} = i\omega \varepsilon_0 \varepsilon_R \left. \frac{\partial \delta \phi_E}{\partial x} \right|_{x=L} = i\omega \varepsilon_0 \varepsilon_R e^{i\omega t} F \left(\sum_{\alpha=1,2} ik_\alpha \Pi_\alpha \Gamma'_\alpha(L) + \Phi' \right). \quad (51)$$

3.2.2 Dispersion Relation

The relation between the wave-numbers k_α and the frequency ω is called dispersion relation. We find this expression with the eigenvalues λ_α of the matrix \mathcal{A} , see eq. (42). The analytic solution is presented in sec. SI-5 A. We illustrate the dispersion relation and both eigenvectors for LP30 electrolyte in fig. 2. Here, a distinct physical meaning emerges for each wave number/eigenvector pair at frequencies below a transition frequency. We identify this frequency as $f_{\text{trans}} = \frac{\kappa}{2\pi \varepsilon_0 \varepsilon_R}$ which lies between $10^6 - 10^8$ Hz for reasonable parameters. For all frequencies f below this value we find that k_2 aligns with k , the wave number of the neutral solutions given by eq. (17). Simultaneously, η_2 attains the constant value $n_+/n_- = -z_-/z_+$. Therefore, $\vec{\eta}_2 \Gamma_2$ describes charge-neutral salt concentration oscillations on the system scale. This eigenvalue/vector-pair is referred to as the ‘‘far-field’’ eigenvalue/vector-pair.

In contrast, $\text{imag } k_1$ quickly attains a constant value below the critical frequency f_{trans} . We refer to the in-

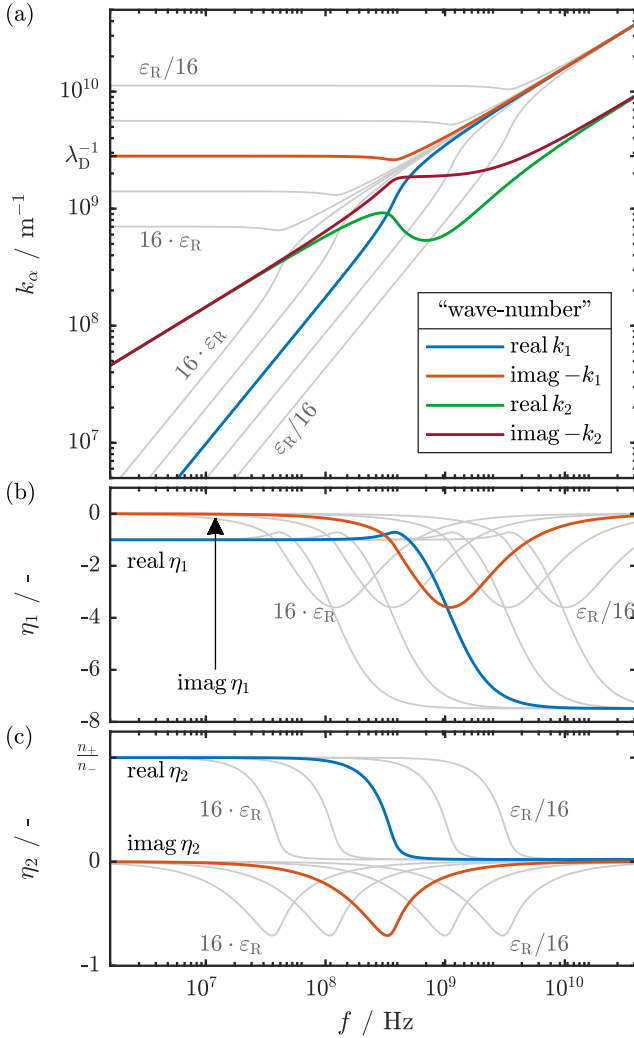


Figure 2: Frequency dependence of k_α and η_α for a monovalent salt (LiPF₆ EC/DMC). The parameters used are listed in table SI-1. The grey lines illustrate the dependence on ϵ_R which we change in multiples of 4 around the base value, i.e., $\epsilon_R = 1.96, 7.85, 31.41, 125.6,$ and 502.6 .

verse of this value ($|k_1|^{-1}$) as the double layer length λ_{DL} . This quantity is typically equal to a few Å in standard lithium-ion batteries. We obtain this value by evaluating k_1 at $\omega = 0$ (see sec. SI-5 B),

$$\lambda_{DL} = \sqrt{-\frac{\epsilon_0 \epsilon_R RT}{z_+ z_- F^2} \frac{\mathcal{N} \mathcal{F}_{salt}}{c_{salt}} \gamma (1 - \gamma)}. \quad (52)$$

The value of η_1 at frequencies below f_{trans} corresponds to a non-electroneutral electrolyte. Therefore, $\bar{\eta}_1 \Gamma_1$ describes diffuse and charged double layers which decay exponentially with λ_{DL} . Solutions of this eigenvalue/vector-pair become only relevant near the interfaces and are referred to as “near-field” solutions below.

Electrochemical impedance measurements are usually not performed with frequencies larger than 10^6 Hz. This means that all experimentally relevant frequencies are

smaller than f_{trans} . The relative permittivity does not depend on the frequency in this frequency range as well. For instance, in the case of ethylene carbonate, ϵ_R begins to change at frequencies larger than 10^9 Hz.⁵⁴ We therefore conclude that $\eta_1, \eta_2,$ and $k_1 = -i\lambda_{DL}^{-1}$ are constant in the relevant frequency range. Additionally, k_2 can be approximated by k , see eq. (17).

3.2.3 Real Double Layer and Interface Capacity

An important distinction that sets our model apart from other similar models is the non-ideal electrolyte that we consider. Non-ideal behaviour is captured by the thermodynamic coefficient \mathcal{F}_{salt} and the asymmetry factor γ , see eq. (SI-51a). Additionally, we consider ionic interactions and ionic association with the Onsager matrix, specifically the transference numbers. However, our theory does not consider the finite size of individual ions and molecules. This can result in a wrong prediction of the double layer thickness λ_{DL} . We take such errors into account by manually adjusting λ_{DL} with the dimensionless parameter ζ

$$\lambda_{DL} \rightarrow \zeta \cdot \lambda_{DL}, \quad \text{and} \quad \hat{\lambda}_{DL} \rightarrow \zeta \cdot \hat{\lambda}_{DL}. \quad (53)$$

This modification adjusts the double layer capacity C_I which determines f_I , the resonance frequency of the interface reaction, see eq. (75).

In realistic systems, C_I includes capacitive contributions from a layer of specifically adsorbed ions. However, such a layer is not considered in our model, see eq. (59). Equation (53) also corrects for this simplification.

Our impedance model assumes a reference state without a diffuse layer at the interface. This is similar to the assumption that the electrodes are polarized to the potential of zero charge and requires that the electrodes are polarized to a specific potential. If the electrodes are polarized to any other potential, charged double layers will be part of the reference state. These double layers become several nm thick in ionic liquids.¹⁸ In this scenario, our theory does not predict the double-layer thickness correctly.

In conclusion, some model simplifications result in the incorrect prediction of f_I , the resonance frequency of the interface reaction. We use eq. (53) in sec. 5 for comparing our model with experimental impedance data.

3.2.4 Interface Reaction

The interface reaction is driven by the linearized overpotential given in eq. (12). This expression depends on the electrochemical potential in the electrolyte

$$\delta\phi^{bulk} = \delta\phi_E^{bulk} + \frac{1}{z_+ F} \frac{\partial \mu_+}{\partial c_+} \delta c_+^{bulk}. \quad (54)$$

In electroneutral models, we evaluate these quantities directly at the interface as these theories do not resolve

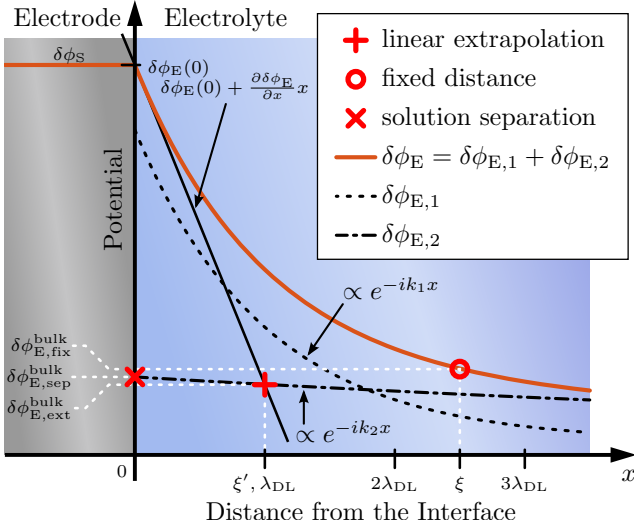


Figure 3: Illustration of the potential deviation close to the interface with three methods to determine $\delta\phi_E^{\text{bulk}}$. The red line shows the spatial dependence of $\delta\phi_E$ which can be separated into two contributions $\delta\phi_E = \delta\phi_{E,1} + \delta\phi_{E,2}$. The spatial dependence of these parts is given by e^{-ik_1x} and e^{-ik_2x} respectively, see eqs. (44) and (46). For illustrative purposes, k_2 has been chosen equal to $k_1/10$.

charged double layers. As illustrated in fig. 3, charged double layers can contribute significantly to the concentration and potential deviation despite being only a few Å thick.⁵⁵ The combination of a Butler-Volmer rate expression and a locally electroneutral electrolyte is a well established method. Therefore, agreement with the neutral theory is a prerequisite for the non-neutral model. This can only be achieved if the double layer contributions to concentration and potential deviation in eq. (54) are not included in the definition of the “bulk” values. Figure 3 illustrates three methods which achieve this:

1. *Fixed distance:* We can evaluate the deviation variables at a fixed distance ξ in front of the interface

$$\delta\phi_{E,\text{fix}}^{\text{bulk}} = \delta\phi_E(\xi). \quad (55)$$

This has two disadvantages. First, an additional parameter ξ is introduced by this definition. Note that the bulk values are used to define the overpotential which is in turn used to express the reaction rate. This reaction rate is used in the flux boundary condition at the interface. Then, the boundary conditions depend on variables which are not evaluated at the boundary itself.

2. *Linear extrapolation:* This problem can be bypassed by using linear extrapolation to obtain the bulk value

$$\delta\phi_{E,\text{ext}}^{\text{bulk}} = \delta\phi_E(0) + \xi' \cdot \left. \frac{\partial\delta\phi_E}{\partial x} \right|_{x=0}. \quad (56)$$

In this method, both the deviation variable and its derivative are evaluated at the interface. Note that this definition also requires one additional parameter ξ' .

3. *Solution separation:* This method can be used if the deviation variable can be uniquely decomposed into a part that describes the diffuse layer in front of the interface and a bulk contribution. Then, the near-field contribution can be subtracted from the value at the interface to obtain the far-field value

$$\delta\phi_{E,\text{sep}}^{\text{bulk}} = \delta\phi_E(0) - \delta\phi_{E,1}(0) = \delta\phi_{E,2}(0). \quad (57)$$

The advantage of this definition over the other methods is that no additional interface length ξ has to be defined. It also clearly connects to neutral models.

Figure 3 illustrates that the bulk values $\delta\phi_{E,\text{fix}}^{\text{bulk}}$, $\delta\phi_{E,\text{ext}}^{\text{bulk}}$, and $\delta\phi_{E,\text{sep}}^{\text{bulk}}$ nearly coincide for a reasonable choice of the additional parameters. Here, we assume $\xi \gg \lambda_{\text{DL}}$ for the first method and $\xi' = \lambda_{\text{DL}}$ for the second method.

As discussed in sec. 3.2.2, our solution is clearly divided into a near-field and a far-field part in the relevant frequency range. We therefore use the solution separation method which yields simple expressions for the boundary values, simplifying the analytical calculations,

$$\vec{\delta c}^{\text{bulk}} = e^{i\omega t} \vec{\eta}_2 \Gamma_2(L), \quad (58a)$$

$$\delta\phi_E^{\text{bulk}} = e^{i\omega t} F (\Pi_2 \Gamma_2(L) + \Phi' L + \Phi). \quad (58b)$$

In the neutral system we connect electrode and electrolyte potential with the rate expression, see eq. (23). This is possible because the reaction rate j_I is equal to I , the external current between the electrodes. However, in the non-neutral system charge can accumulate in the diffuse layer and in the double layer screening charge Q_S , see sec. 3.2.1. Then, I is equal to $j_I + j_S$ and a new equation is needed to relate electrode and electrolyte potential. We assume that the potential deviation is a continuous function of space so that

$$\delta\phi_S^+ = \delta\phi_E(L). \quad (59)$$

This is illustrated in fig. 3. Most theories of the electrochemical double layer consider a diffuse layer and a layer of specifically adsorbed ions.⁵⁰ Specifically adsorbed ions have at least partially lost their solvation shell and are in direct contact with the interface. This layer can have a net charge and a dipole moment. By using eq. (59) we neglect the dynamics of these quantities.

Modeling the dynamics of the inner Helmholtz plane is beyond the scope of this work. An interested reader is referred to dedicated works on this subject.⁵⁶

We now express the linearized overpotential η_{lin} , see

eq. (12), with eqs. (54), (58) and (59)

$$\eta_{\text{in}} = e^{i\omega t} \left(F \Pi_1 \Gamma_1(L) - \frac{\eta_2}{z_+ F} \frac{\partial \mu_+}{\partial c_+} \Gamma_2(L) \right). \quad (60)$$

Here, we consider the simple concentration dependence of the chemical potentials given by eq. (4). We introduce the dimensionless parameter γ to connect \mathcal{F}_+ with $\mathcal{F}_{\text{salt}}$ in sec. SI-3 A

3.2.5 Solution without Solid Electrolyte Interphase

In this subsection, we discuss the cell without SEI. This means that the electrolyte spans from $-L$ to L and is in direct contact with the electrode. We use the symmetry argument to eliminate three of the six coefficients which define the general solution

$$C_1 = C_1^+ = -C_1^-, \quad (61a)$$

$$C_2 = C_2^+ = -C_2^-, \quad (61b)$$

$$\Phi = 0. \quad (61c)$$

$$\mathbf{S} = - \begin{pmatrix} \Omega_{+1} \cdot 2 \cos(k_1 L) & \Omega_{+2} \cdot 2 \cos(k_2 L) & \frac{t+\kappa}{z_+} \\ \Omega_{-1} \cdot 2 \cos(k_1 L) & \Omega_{-2} \cdot 2 \cos(k_2 L) & \frac{t-\kappa}{z_-} \end{pmatrix} + \frac{1}{\mathcal{R}} \begin{pmatrix} \frac{1}{z_+} \left(1 - \frac{\rho_+}{\rho}\right) & 0 & 0 \\ 0 & \frac{1}{z_-} \frac{\rho_+}{\rho} & 0 \end{pmatrix} \begin{pmatrix} \Pi_1 \cdot 2i \sin(k_1 L) & -\frac{\eta_2}{z_+ F^2} \frac{\partial \mu_+}{\partial c_+} \cdot 2i \sin(k_2 L) & 0 \\ \Pi_1 \cdot 2i \sin(k_1 L) & -\frac{\eta_2}{z_+ F^2} \frac{\partial \mu_+}{\partial c_+} \cdot 2i \sin(k_2 L) & 0 \\ 0 & 0 & 0 \end{pmatrix}. \quad (64)$$

3.2.6 Solution with Solid Electrolyte Interphase

Next, we transfer the solution of the non-neutral electrolyte to the porous SEI which spans from $x = L'$ to $x = L$. To account for the morphology of the SEI, we use the effective transport parameters introduced in sec. 2.4. However, the porosity of the SEI phase also appears in a few specific steps during the calculation. It enters the Poisson equation,

$$-\frac{\varepsilon \rho}{\varepsilon_0 \varepsilon_{\text{R}}} = \Delta \delta \phi_{\text{E}}. \quad (65)$$

Here, we replace the charge density in the pores with the averaged charge density in the SEI. Additionally, we introduce $\hat{\varepsilon}_{\text{R}}$, the mean permittivity of the SEI. The porosity also appears in the mass balance equation. Considering these changes, the modified version of eq. (39) becomes

$$\partial_t \vec{\delta c} = \varepsilon^{-1} \hat{\mathbf{D}}^* \Delta \vec{\delta c} - \hat{\mathcal{T}}^* \vec{\delta c}. \quad (66)$$

We calculate $\hat{\mathbf{D}}^*$ and $\hat{\mathcal{T}}^*$ in the same way as in the electrolyte phase but use the effective transport parameters for the SEI phase. However, $\varepsilon^{-1} \hat{\mathbf{D}}^*$ instead of \mathbf{D}^* is

As a result, the functions Γ_α and Γ'_α become common trigonometric expressions

$$\Gamma_\alpha = 2i C_\alpha \sin(k_\alpha x), \quad (62a)$$

$$\Gamma'_\alpha = 2C_\alpha \cos(k_\alpha x). \quad (62b)$$

We insert these functions into the flux expression eq. (48) and the equation for the interface reaction rate eqs. (11) and (60). Next, both of these quantities are used to write the flux boundary conditions given by eq. (14). This results in two homogeneous linear equations in the remaining coefficients C_1, C_2, Φ' . We write them in matrix form

$$\mathbf{S} \vec{C} = 0, \quad (63)$$

where $\vec{C} = (C_1, C_2, \Phi')^T$ is the coefficient vector and \mathbf{S} is a 2x3 matrix given by eq. (64). Equation (63) determines \vec{C} with respect to its amplitude. We give the analytic solution in the SI, see eq. (SI-79). This solution defines all quantities in eq. (1), i.e., ϕ_{S}^+ , j_{I} , and j_{S} with eqs. (11), (46), (59) and (60). We therefore use eq. (1) to calculate Z analytically, see eq. (SI-80).

used for the calculation of \hat{k}_α and $\hat{\eta}_\alpha$. The modified Poisson equation eq. (65) also affects the definition of $\hat{\Pi}_\alpha$,

$$\hat{\Pi}_\alpha = \frac{\varepsilon (z_+ \hat{\eta}_\alpha + z_-)}{\varepsilon_0 \varepsilon_{\text{R}} \hat{k}_\alpha^2}. \quad (67)$$

The SEI specific set of transport parameters, eigenvalues, and eigenvectors $(\hat{k}_\alpha, \hat{\eta}_\alpha)$ is used in the definition of $\hat{\Gamma}_\alpha(x)$. We then find the frequency dependent solutions of concentration and potential deviation

$$\vec{\delta c} = e^{i\omega t} \cdot \begin{cases} \sum_\alpha \vec{\eta}_\alpha \Gamma_\alpha & x \leq L' \\ \sum_\alpha \vec{\eta}'_\alpha \hat{\Gamma}_\alpha & x \geq L' \end{cases}, \quad (68a)$$

$$\delta \phi_{\text{E}} = e^{i\omega t} F \cdot \begin{cases} \sum_\alpha \Pi_\alpha \Gamma_\alpha + \Phi' \cdot x & x \leq L' \\ \sum_\alpha \hat{\Pi}_\alpha \hat{\Gamma}_\alpha + \hat{\Phi}' \cdot x + \hat{\Phi} & x \geq L' \end{cases} \quad (68b)$$

for x between 0 and L . Compared to the system without SEI, six additional coefficients need to be determined. Consequently, we consider six additional boundary conditions.

1. Both $\vec{\delta c}$ and $\delta \phi_{\text{E}}$ are continuous $x = L'$.

2. The particle fluxes N_+ and N_- are continuous at $x = L'$.
3. No charge is stored at the interface between the electrolyte and the SEI phase and Gauss's law implies $\epsilon_R \partial_x \delta \phi_E(L') = \hat{\epsilon}_R \partial_x \delta \hat{\phi}_E(L')$

These six additional equations are linear in the coefficients. We write them in matrix form with the expanded coefficient vector $\vec{C} = (C_1, C_2, \Phi', \hat{C}_1^+, \hat{C}_1^-, \hat{C}_2^+, \hat{C}_2^-, \hat{\Phi}', \hat{\Phi})^T$. This results in the 8x9 matrix $\hat{\mathcal{S}}$ if the two flux boundary conditions at $x = L$ are considered, see eq. (14). We denote this matrix in the SI in sec. SI-5 D. The coefficient vector must satisfy

$$\hat{\mathcal{S}}\vec{C} = 0. \quad (69)$$

Because of the increased size of the system of equations we do not perform this calculation analytically. Instead, we solve eq. (69) numerically to obtain the coefficient vector \vec{C} for each frequency of interest. We then use this result in the expressions for $\delta \phi_E$, j_I , and j_S , to calculate the impedance Z with eq. (1).

4 Discussion

In this section we analyze and discuss the impedance models derived in the previous section. We first discuss the models without SEI and compare the differences between the neutral and non-neutral approach in sec. 4.1. The impedance models with SEI are then discussed in sec. 4.2. An essential part of our analysis is the approximation and simplification of the non-neutral models. Our simplified models bring out the parameter dependence of the impedance signal over a large parameter range. The corresponding equivalent circuits are discussed in sec. 4.3.

4.1 Impedance - Without SEI

Figure 4 shows the impedance of the half-cell without SEI. It consists of three distinct features, for both, the neutral and the non-neutral model, namely

- the resistance of the electrolyte R_E/Z_E ,
- the interface resistance R_I/Z_I ,
- the polarization impedance R_D/Z_D .

We label real impedance contributions that do not depend on frequency with R . In contrast, complex impedance contributions that depend on frequency are labelled with Z . Our neutral model does not predict the frequency dependence of electrolyte and interface resistance. However, neutral models give the polarization impedance Z_D in sec. 4.1.1. The frequency dependent impedance of interface reaction Z_I and electrolyte Z_E are discussed with our non-neutral model in sec. 4.1.2.

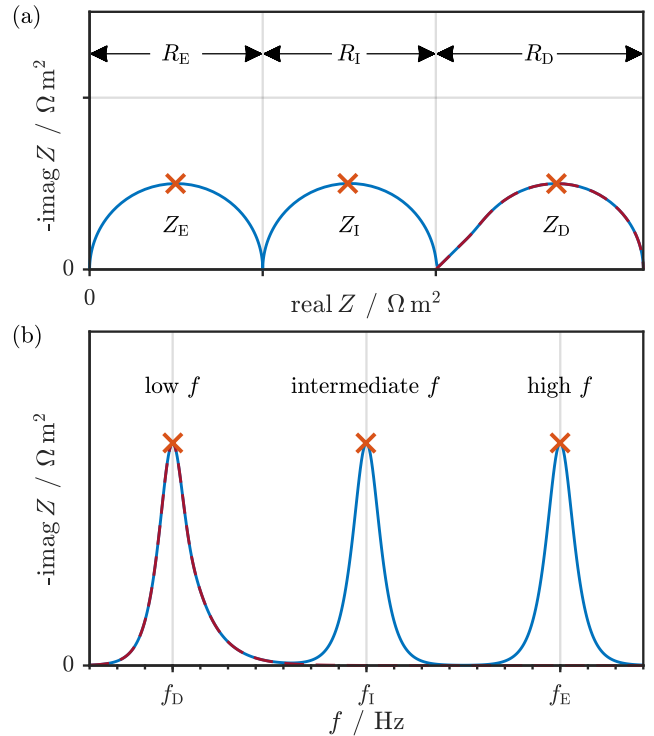


Figure 4: Schematic impedance spectrum of the symmetric cell without SEI. (a) Nyquist plot. (b) Bode plot. The solid blue line shows the impedance of the non-neutral model whereas the dashed red ones show the impedance of the neutral one. Crosses mark the resonance frequencies.

4.1.1 Diffusion Impedance

The neutral impedance without SEI is given by eqs. (24) and (25). The assumption of local electroneutrality is incompatible with charge accumulation at the interface. Therefore, the only complex and frequency dependent impedance contribution in the neutral model is the diffusion resistance

$$Z_D = R_D \frac{\tan(kL)}{kL}. \quad (70)$$

This function is illustrated in fig. 5a, R_D is given by eq. (25c). Z_D describes the impedance increase of the electrolyte as salt concentration gradients emerge at low frequencies. We illustrate these salt concentration gradients for different frequencies in fig. 5b. The label Z_D denotes that this process is governed by salt diffusion. In literature, it is referred to as a diffusion, Warburg Short (W_S), and finite-length Warburg impedance. R_D , the amplitude of this effect is determined by numerous parameters, namely the distance between the electrodes L , the transference number t_- , and the salt diffusion coefficient D_{salt}^* . Note that t_- is referenced to the center-of-mass velocity, whereas D_{salt}^* is an apparent parameter as defined in sec. 2.2. R_D is proportional to $\frac{d\mu_{\text{salt}}}{dc_{\text{salt}}}$ which depends on the salt concentration c_{salt} and the thermodynamic factor $\mathcal{F}_{\text{salt}}$. The relative cation density ρ_+/ρ appears as correction of the transference number t_- in

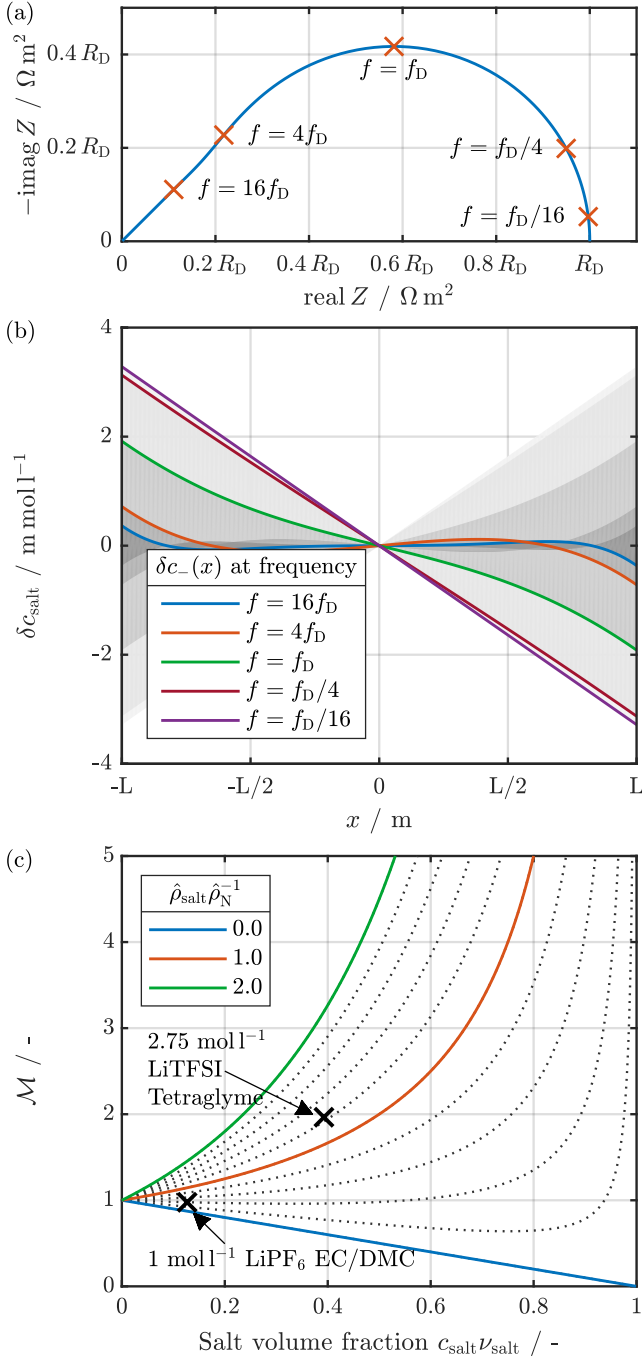


Figure 5: (a) Illustration of the finite-length Warburg impedance. (b) Envelopes of the salt concentration profile in the cell for five different frequencies marked in part (a). The profiles are obtained for the LP30 electrolyte with a current density of $I_0 = 10 \mu\text{A cm}^{-2}$. Parameters are listed in table SI-1. (c) The factor \mathcal{M} is a function of $c_{\text{salt}} \nu_{\text{salt}}$, see eq. (26). \mathcal{M} scales R_D , the amplitude of the diffusion impedance, see eq. (25c). Parameters to calculate the marked values are listed in table SI-1.

concentrated electrolytes. Additionally, R_D is proportional to the factor $\mathcal{M} = \rho^2 \hat{\rho}_{\text{N}}^{-1} \tilde{\rho}_{\text{N}}^{-1}$ which is rewritten in eq. (26). \mathcal{M} is equal to 0.977 and 1.965 for the LP30 and LiTFSI electrolyte, see table SI-1. We illustrate

this factor in fig. 5c, showing that it diverges if the salt concentration reaches its theoretical maximum. It approaches unity for dilute solutions. In conclusion, the amplitude of the diffusion resistance has a complex parameter dependence.

In contrast, we find that the frequency dependence of Z_D is simply given by the frequency dependence of k , see eq. (17). The wave number k depends only on D_{salt}^* , the apparent salt diffusion coefficient. The characteristic timescales of the diffusion impedance Z_D also depend on L , the distance between the electrodes. We calculate the resonance frequency of Z_D numerically and obtain the following approximation

$$f_D \approx \frac{1.2703 D_{\text{salt}}^*}{\pi L^2}. \quad (71)$$

Figure 5b illustrates the oscillations in the concentration profiles at various frequencies close to f_D .

Z_D is typically not observed in modern batteries or test cells. It is covered by other contributions such as diffusive processes in intercalation electrodes. Therefore, Z_D is best observed if non-intercalation electrodes are used, i.e., metallic lithium. Another challenge in measuring Z_D are the low frequencies that have to be considered (sub mHz). Such measurements take a long time and require great care to avoid the initial state from being perturbed. f_D can be shifted towards higher values by reducing the distance between the electrodes, see eq. (71). However, this reduces the amplitude of the effect.

4.1.2 Electrolyte and Interface Impedance

Our neutral models predict a real valued and frequency independent resistance for electrolyte and interface (R_E and R_I), see eqs. (25a) and (25b). We therefore use the non-neutral impedance model without SEI, see sec. 3.2.5, to discuss Z_E and Z_I . The full expression for Z is given by eq. (SI-80). In contrast to the electroneutral case, both, the resistance of the electrolyte Z_E and the interface resistance Z_I , are frequency dependent. Their Nyquist plots have the common semicircle shape, see fig. 4.

The full expression for Z is too intricate for a direct analysis. However, we find a simplified approximation when three conditions are met. Firstly, the distance between the electrodes is larger than the double layer thickness, i.e., $L \gg \lambda_{\text{DL}}$. Secondly, the interface reaction is parametrized such that its resonance frequency f_I is smaller than $f_{\text{trans}} = \frac{\kappa}{2\pi\epsilon_0\epsilon_R}$, see sec. 3.2.2. We show below that these assumptions are equivalent to $\mathcal{R} \gg \lambda_{\text{DL}}/\kappa$. This allows us to approximate k_1 , η_1 , and η_2 as constants as discussed in sec. 3.2.2. Finally, we assume $f_D \ll f_E$ which allows us to approximate eq. (SI-80) with three distinct contributions,

$$Z(\omega) = Z_E + Z_I + Z_D. \quad (72)$$

The expression we obtain for Z_D aligns with the dif-

fusion resistance derived with the neutral model in sec. 4.1.1. Z_E and Z_I are given by

$$Z_E = \frac{L}{\kappa + i\omega\epsilon_0\epsilon_R}, \quad (73a)$$

$$Z_I = \frac{\lambda_{DL}}{\lambda_{DL}/\mathcal{R} + i\omega\epsilon_0\epsilon_R}. \quad (73b)$$

Alternatively, we can derive these expressions with equivalent circuits. Both electrodes form a parallel-plate capacitor filled with electrolyte, a polarizable medium. In parallel to this capacitance, the electrolyte acts as an ohmic resistor. The capacity and ohmic resistance of these elements are equal to $C_E = \epsilon_0\epsilon_R/L$ and $R_E = L/\kappa$. We then obtain eq. (73a) according to Kirchhoff's rule. The resonance frequency of this semicircle is given by

$$f_E = \frac{\kappa}{2\pi\epsilon_0\epsilon_R} = f_{\text{trans}}. \quad (74)$$

Only the conductivity κ and the dielectric constant ϵ_R of the electrolyte influence this frequency. Note that f_E is equal to f_{trans} , see sec. 3.2.2. It marks the transition from the simple low frequency behavior of k_α and η_α to the more complicated high frequency one. It is in the 100 – 1000 MHz range for common parameters, making it too large to be observed in an electrochemical impedance measurement. Consequently, the electrolyte impedance Z_E is typically treated as a constant and purely ohmic contribution.

The interface resistance Z_I corresponds to the charge-transfer reaction. We obtain Z_I with a parallel circuit of the interface capacitance $C_I = \epsilon_0\epsilon_R/\lambda_{DL}$ (see eq. (SI-74)) and the interface resistance $R_I = \mathcal{R}$. The resonance frequency of the interface reaction is equal to

$$f_I = \frac{\lambda_{DL}}{2\pi\epsilon_0\epsilon_R\mathcal{R}} \quad (75)$$

and depends on λ_D , ϵ_R , and \mathcal{R} . The complex parameter dependence of the double layer thickness λ_{DL} is given in eq. (52). We discuss eventual shortcomings and corrections of this prediction in sec. 3.2.3.

The agreement between the sum of the three simplified expressions and the full expression for Z is excellent. It is retained even if the resonance frequencies of the interface reaction and the diffusion impedance overlap. Differences between our simplification and the full expression become relevant if the electrodes are less than $10\lambda_{DL} \sim 5$ nm apart. Furthermore, we observe deviations if f_I or f_D are larger than $f_E/10$. Such conditions do not appear in standard battery cells. To conclude, the impedance without SEI is given by two conventional semicircles and the Warburg diffusion element which is derived with the neutral model.

4.2 Impedance - With SEI

The presence of the SEI complicates the impedance calculation so that an analytical solution of the non-neutral

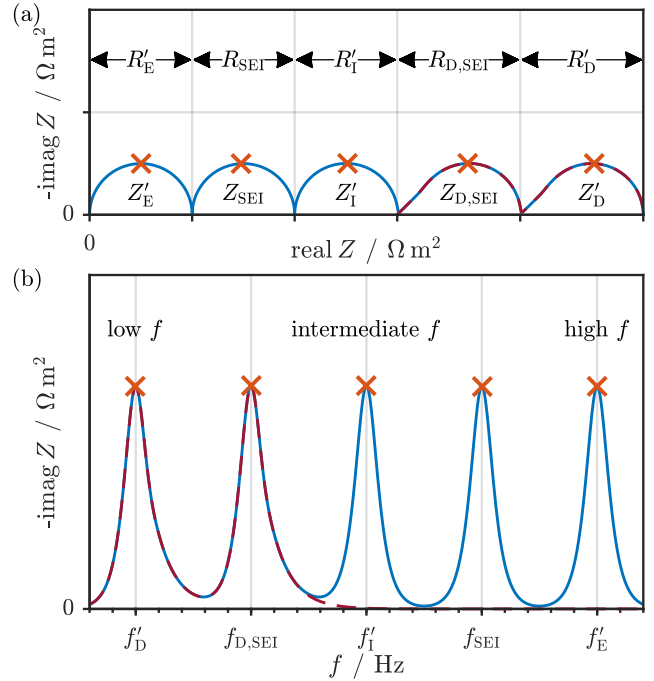


Figure 6: Schematic impedance spectrum of the symmetric cell with SEI. (a) Nyquist plot. (b) Bode plot. The solid blue line shows the impedance of the non-neutral model whereas the dashed red ones show the impedance of the neutral one. Crosses mark the resonance frequencies.

impedance is no longer feasible. Therefore, this model is only solved numerically. However, we find that it is well approximated by the sum of five distinct impedance contributions,

$$Z(\omega) = Z'_E + Z_{SEI} + Z'_I + Z_{D,SEI} + Z'_D. \quad (76)$$

We illustrate this result in fig. 6. It shows that the SEI adds two impedance features to our model. One semicircle represents the ionic transport resistance of the surface film which we label Z_{SEI} . Furthermore, a second diffusion resistance, $Z_{D,SEI}$, appears. This is a consequence of modeling charge transport through the SEI with a liquid electrolyte. Liquid electrolytes allow the formation of concentration gradients as opposed to solid electrolytes. All three remaining impedance contributions in eq. (76) are marked with a '. This indicates that the expressions given in sec. 4.1 must be adjusted to account for the slightly modified geometry ($L \rightarrow L'$).

4.2.1 Electrolyte and Interface Impedance

We revisit the impedance contributions in eq. (76) that appear in the impedance model without SEI, see sec. 4.1. The presence of SEI reduces the size of the electrolyte phase. It is now given by $L' = L - \hat{L}$ where \hat{L} is the thickness of the SEI. We consider this and modify

the expression for the electrolyte resistance

$$R'_E = \frac{L'}{\kappa}, \quad \text{and} \quad Z'_E = \frac{L'}{\kappa + i\omega\epsilon_0\epsilon_R}. \quad (77)$$

This change does not affect the corresponding resonance frequency, $f'_E = f_E$.

We denote the double-layer thickness in the SEI pores with $\hat{\lambda}_{DL}$. It is different from the double-layer thickness in the bulk electrolyte λ_{DL} . Thus, the expression for the interface impedance becomes

$$Z'_I = \frac{\hat{\lambda}_{DL}}{\hat{\lambda}_{DL}/\mathcal{R} + i\omega\epsilon_0\epsilon_R}, \quad (78a)$$

$$f'_I = \frac{\hat{\lambda}_{DL}}{2\pi\epsilon_0\epsilon_R\mathcal{R}}. \quad (78b)$$

The presence of SEI also affects the diffusion impedance of the electrolyte Z_D . It is replaced by Z'_D which is given by eq. (33a). We discuss this in sec. 4.2.3.

4.2.2 SEI Impedance

Z_{SEI} describes the ionic impedance of the SEI. In analogy to sec. 4.1.2, we find a good approximation for this expression with an equivalent circuit. To this aim we model the SEI as a parallel circuit consisting of a capacitor and an ohmic resistance,

$$C_{SEI} = \frac{\epsilon_0\hat{\epsilon}_R}{\hat{L}}, \quad \text{and} \quad R_{SEI} = \frac{\hat{L}}{\hat{\kappa}}. \quad (79)$$

The capacitive and ohmic impedance contribution depends on the SEI thickness \hat{L} , the conductivity $\hat{\kappa}$, and the relative permittivity $\hat{\epsilon}_R$. This corresponds to the common assumption that SEI resistance depends mostly on its thickness.^{57,58} We then obtain

$$Z_{SEI} = \frac{\hat{L}}{\hat{\kappa} + i\omega\epsilon_0\epsilon_R} = \frac{\hat{L}}{\frac{\epsilon}{\tau}\kappa + i\omega\epsilon_0\epsilon_R} \quad (80)$$

from Kirchhoff's law. The resonance frequency of this semicircle is given by

$$f_{SEI} = \frac{\epsilon\kappa}{2\pi\tau\epsilon_0\hat{\epsilon}_R} = \frac{\epsilon}{\tau} \frac{\epsilon_R}{\hat{\epsilon}_R} f_E. \quad (81)$$

4.2.3 Diffusion Impedance in SEI and Electrolyte

In this section, we discuss and simplify the expressions for the diffusion resistance of the SEI and the electrolyte phase (Z_{SEI} and Z'_D , see eq. (33)). We calculate these expressions with the neutral impedance model in sec. 3.1.3. As discussed in sec. 2.4, we assume that the SEI is nano porous. This implies that the SEI porosity ϵ is small and suggests that the SEI tortuosity τ is large. Therefore, we assume $\frac{\epsilon}{\tau} < \frac{\epsilon}{\sqrt{\tau}} \ll 1$ in the simplifications below. Taking into account that both $|\tan(kL')|$ and $|\tan(\hat{k}\hat{L})|$ are bounded by 1.2 then implies $\Psi \approx 1$, see eq. (34b). This results in an approximate expression

for $Z_{D,SEI}$,

$$Z_{D,SEI} \approx \frac{\hat{L}\Theta}{\hat{D}_{salt}^*} \left(\hat{t}_- - \frac{\rho_+}{\rho} \right)^2 \frac{\tan(\hat{k}\hat{L})}{\hat{k}\hat{L}}. \quad (82)$$

This equation has the same structure as the expression for Z_D derived in sec. 4.1.1. We therefore transfer the results from sec. 4.1.1 and apply them to eq. (82). In this way, we obtain an approximation for the resonance frequency of the SEI diffusion impedance

$$f_{D,SEI} \approx \frac{1.2703\hat{D}_{salt}^*}{\pi\hat{L}^2}. \quad (83)$$

We also use $\Psi \approx 1$ to simplify the electrolyte diffusion impedance Z'_D which is given by eq. (33a). To further simplify this expression, we assume that the resonance frequency of the diffusion resistance in the SEI $f_{D,SEI}$ is larger than the resonance frequency of the diffusion impedance in the electrolyte f_D . This implies that $\sec(\hat{k}\hat{L}) \approx 1$ in the relevant frequency range in eq. (33a), resulting in

$$Z'_D \approx \frac{L'\Theta}{D_{salt}^*} \left(t_- - \frac{\rho_+}{\rho} \right)^2 \frac{\tan(kL')}{kL'}. \quad (84)$$

This is the same expression as the original expression for Z_D in eq. (70), besides the replacement of L with L' . We use this similarity to find the equation for the resonance frequency of Z'_D ,

$$f'_D \approx \frac{1.2703D_{salt}^*}{\pi L'^2}. \quad (85)$$

Equations (84) and (85) are important results. They show that the SEI does not influence electrolyte impedance contributions ($Z'_E \approx Z_E$ and $Z'_D \approx Z_D$), if we consider that the SEI is thin ($L' \approx L$).

Next, we compare the amplitude of $Z_{D,SEI}$ with the amplitude of Z'_D . No approximation is used for this comparison. We divide eq. (33b) by eq. (33a) in the stationary limit $\omega \rightarrow 0$

$$\frac{R_{D,SEI}}{R'_D} = \frac{R_{SEI}}{R_E} \left(\hat{t}_- - \frac{\rho_+}{\rho} \right)^2 \left(t_- - \frac{\rho_+}{\rho} \right)^{-2}. \quad (86)$$

Here, we consider that $\frac{\tau}{\epsilon} \frac{\hat{L}}{L'}$ is equal to $\frac{R_{SEI}}{R_E}$. In most impedance experiments the resistance of the electrolyte R_E is found to be smaller than R_{SEI} , the resistance of the SEI.^{4,33} If we assume $R_{SEI} > R_E$, we obtain the following inequality

$$\frac{R_{D,SEI}}{R'_D} > \left(\hat{t}_- - \frac{\rho_+}{\rho} \right)^2 \left(t_- - \frac{\rho_+}{\rho} \right)^{-2}. \quad (87)$$

Thus, if $\hat{t}_- \gtrsim t_-$ the diffusion impedance of the SEI would be larger than the diffusion impedance of the electrolyte. Because this is not observed in experiments, we conclude that the transference number in the SEI pores is different from the bulk value. Specifically, $\hat{t}_+ = 1 - \hat{t}_-$

must be close to $1 - \rho_+/\rho$ to reduce the amplitude of $Z_{D,SEI}$ such that our theory agrees with experimental observations. Note that this value is close to unity in lithium-ion electrolytes. Large cation transference numbers have been observed in mesoporous systems which immobilize anions.⁵¹ A similar situation could emerge in nano-sized SEI pores. In principle, we could use other parameters such as the thermodynamic coefficient in the SEI to reduce the amplitude of $Z_{D,SEI}$. However, this leads to unreasonable parameter choices because of the quadratic appearance of \hat{t}_- in eq. (25c).

In summary, large transference numbers $\hat{t}_+ \approx 1$ are necessary to avoid contradicting experimental observations. Therefore, charge transport in the SEI has “solid electrolyte character” even if we assume ion transport in a liquid pore space.

4.3 Summary: Equivalent Circuits

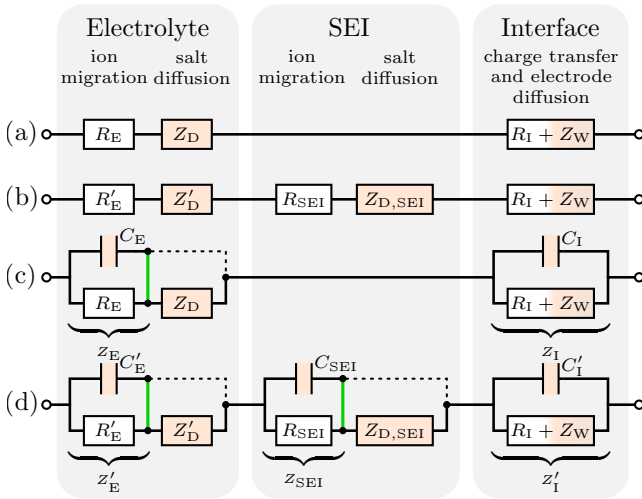


Figure 7: Summary of equivalent circuits. Neutral model (a), neutral model with SEI (b), non-neutral model (c), and non-neutral model with SEI (d). Circuit components with a frequency dependent resistance such as capacitors and Warburg elements are colored. Here, Z_D and $Z_{D,SEI}$ are Warburg Short elements. Warburg Open elements Z_W describe diffusion processes in the electrode, see sec. SI-6. Black dashed lines represent the technically correct circuit, the green connections are approximations which we discuss in sec. 4.3.

We now transcribe eqs. (24), (32), (72) and (76) into equivalent circuits. These circuits are summarized in fig. 7. Our neutral models are equivalent to the circuits shown in figs. 7a and 7b. This is different for non-neutral models. The equivalent circuits shown in figs. 7c and 7d are an excellent approximation of the corresponding models provided the following conditions are met.

Firstly, our model demands that the SEI phase and the electrolyte phase are large compared to the corresponding double layer thickness, i.e., $\hat{L} \gg \lambda'_{DL}$, and

$L' \gg \lambda_{DL}$. This guarantees that diffuse layers do not overlap. We assume this in our interface reaction model.

Secondly, the interface reaction can only be represented as a standard RC element if the double layer width is constant in this frequency range. This width is given by the inverse value of k_1 or \hat{k}_1 . These quantities become constant below the transition frequency f_{trans} , see fig. 2. This transition coincides with the resonance frequency of the electrolyte semicircle. Therefore, our analysis requires $f_I \ll f_E$ or $\mathcal{R} \gg \lambda_{DL}/\kappa$.

Equations (72) and (76) are based on the green wiring in figs. 7c and 7d. These approximations are valid if certain resonance frequencies are well separated, i.e., $f_D \ll f_E$, $f'_D \ll f'_E = f_E$, or $f_{D,SEI} \ll f_{SEI}$. This assumption separates the impedance into several distinct contributions. The dotted alternatives do not require these assumption, but they result in a single convoluted impedance expression instead.

5 Validation with Experiments

We now compare our impedance model to the experiment performed by F. Wohde et al.³³ They measured the impedance of a symmetric Li-metal cell with planar electrodes. The measurements were performed in a custom cell that allowed varying the distance between the electrodes. After flooding the cell, its impedance was measured continuously in the high to intermediate frequency range. In this way, the interface resistance was probed during the initial formation of the SEI. It became constant after 24–48 hours, indicating that stable surface films had formed. Impedance measurements were performed only after this time.

We use the impedance data for the Li-TFSI electrolyte in a tetraglyme (G4) solution. The Li-TFSI concentration of the electrolyte was equal to $c_{salt} = 2.75 \text{ mol l}^{-1}$. Measurements were performed for electrode distances of 130, 150, 290, and 330 μm . The impedance data is shown in fig. 8. At first glance, four distinct features can be identified:

Firstly, the ohmic resistance of the electrolyte R_E is equal to 7.5, 8.8, 17.6, and 19.3 Ω , increasing in proportion to the distance between the electrodes. This contribution is subtracted from the data shown in fig. 8. In this way, all remaining features align in the figure.

Secondly, the high frequency semicircle observed in these measurements is not influenced by the electrode distance. Therefore, only interfacial processes like charge transfer reaction Z_I or the SEI resistance Z_{SEI} can be assigned to this resonance. A closer investigation reveals that this semicircle is depressed, suggesting that it contains at least two of these resonances which overlap in frequency space. These processes occur between 30 and 3000 Hz and contribute approximately 250 Ω .

Thirdly, a small impedance contribution of approximately 30 Ω is present in the intermediate frequency range between 10 and 0.1 Hz. This resonance slightly overlaps with other resonances such that we cannot dis-

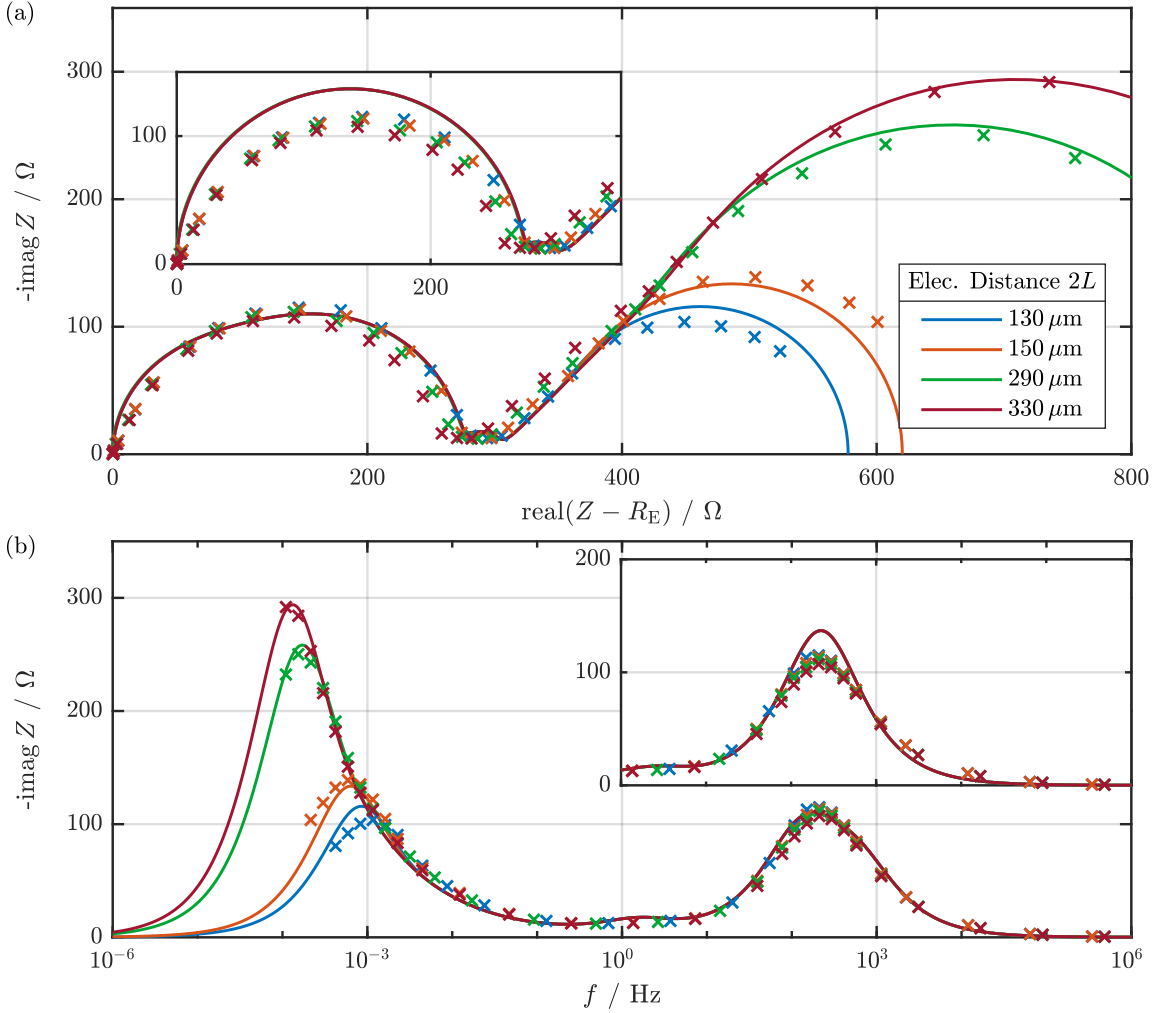


Figure 8: (a) Nyquist plot. (b) Bode plot, the x -axes of the inset aligns with the main x -axes. Both plots show the impedance of a symmetric Li-Li cell with a Li-TFSI tetraglyme electrolyte. Crosses mark experimental data points measured by Wohde et al.³³ Solid lines show our simplified impedance model according to eq. (76). The main sets show this model with parameter set I whereas parameter set II is used in the insets. Both parameter sets are listed in tables SI-1 and SI-2.

tinguish whether it has a semicircle or a Warburg type shape. Due to its low frequency, only Z_I and $Z_{D,SEI}$ are reasonable candidates. We conclude this because the amplitude of this resonance does not scale with the electrode distance. Additionally, typical resonance frequencies of the SEI are much larger, such that only these two candidates remain.

Fourthly, the measurements contain a diffusion type impedance contribution at very low frequencies (10^{-4} – 10^{-3} Hz). Its amplitude scales linearly with the electrode distance so that it can be identified as Z_D .

In conclusion, Z_D can be directly identified in these measurements. Assigning Z_{SEI} , Z_I , and $Z_{D,SEI}$ to the features observed in the experiment is not as simple. We suggest two different parametrizations of the impedance model for this reason. Figure 8 shows the main parametrization in the outer plot and the alternative parametrization in the insets. Let us first discuss parameters that these two options share.

The impedance model itself is over-parametrized.

This means that an impedance measurements alone is insufficient to determine each parameter of the model. Instead, a subset of parameters must be known from independent experiments so that the remaining parameters can be identified. Not all parameters are experimentally accessible. For instance, the porosity ε and tortuosity τ of the SEI. These parameters are chosen as $\varepsilon = 0.1$ and $\tau = 3450$. Note that these parameters and the SEI thickness \hat{L} determine R_{SEI} , the resistance of the SEI see eq. (79). Then, according to eq. (81), the only parameter remaining to tune the corresponding resonance frequency is $\hat{\varepsilon}_R$.

The resistance of the interface reaction is defined by the parameter \mathcal{R} . Originally, the model predicts that the corresponding resonance frequency is determined by \mathcal{R} and λ_{DL} which depends on \mathcal{F}_{salt} , ε_R and γ , see eqs. (SI-71) and (75). As discussed in sec. 3.2.3, model simplifications can lead to an incorrect prediction of the interface capacitance in real systems. We consider this by adjusting the double layer thickness with the dimen-

sionless parameter ζ , see eq. (53). In principle, λ_{DL} could also be adjusted with other model parameters such as $\mathcal{F}_{\text{salt}}$, see eq. (SI-71). However, this would lead to inconsistencies with other impedance contributions.

As mentioned above, we identify the diffusion impedance Z'_D clearly in the experiment. The resonance frequency of this effect is equal to 1.16, 0.59, 0.15, and 0.11 mHz for the four different electrode distances. From this we obtain D_{salt}^* by inverting eq. (71) and averaging the four results, resulting in $D_{\text{salt}}^* = 8.8 \cdot 10^{-12} \text{ m}^2 \text{ s}^{-1}$. We estimate the partial molar volumes of the electrolyte with literature data for a different salt concentration.⁵⁹ R_D , the amplitude of Z_D is then used to identify another parameter, see eq. (25c). At this point, only the thermodynamic coefficient $\mathcal{F}_{\text{salt}}$ and the transference number t_+ are unknown. Typically, $\mathcal{F}_{\text{salt}}$ can be measured independently, e.g., in a concentration cell experiment. However, data for $\mathcal{F}_{\text{salt}}$ is not available in literature for the highly concentrated solution at hand. We use a different approach for this reason. The transference number is taken from^{33,60} which is calculated as follows

$$t_+ = \frac{R_E}{R_E + R_D} = 0.0245. \quad (88)$$

As discussed by Doyle and Newman,⁶¹ this equation correctly gives the transference number for a dilute/ideal electrolyte. Note that neither of these assumptions are applicable to this system. After choosing t_+ , we calculate the thermodynamic factor with the impedance data resulting in $\mathcal{F}_{\text{salt}} = 6.2$. The large thermodynamic factor illustrates the non-ideal behavior of the system. This implies that eq. (88) gives a flawed estimate for the transference number. However, this uncertainty could be removed by measuring the thermodynamic factor independently⁶² and using the impedance measurement to determine the transference number.

We now elaborate on the differences between both parameter sets. They are summarized in the SI, see tables SI-1 and SI-2.⁶³ In our *main* parametrization, both Z_{SEI} and Z_I overlap and form the high frequency semicircle. R_{SEI} and R_I , the resistances of the SEI and the interface reaction are determined by choosing \hat{L} and \mathcal{R} . With the choice listed in table SI-1, these contributions amount to $R_{\text{SEI}} = 102 \Omega$ and $R_I = 168 \Omega$. The resonance frequencies are then adjusted with the choices $\zeta = 5$ and $\hat{\epsilon}_R = 131$. Then, $Z_{D,\text{SEI}}$ must be assigned to the intermediate resonance. At this point, \hat{t}_+ is the only parameter left to scale this impedance contribution. The model fits well to the data if we choose $\hat{t}_+ = 0.9$.

In the *alternative* parametrization, we attribute the high frequency resonance to Z_{SEI} alone. To this aim, we increase R_{SEI} by increasing the SEI thickness to 67 nm. Then, the SEI resistance accounts for $R_{\text{SEI}} = 273 \Omega$. At the same time we adjust the relative permittivity of the SEI to move this semicircle to the correct resonance frequency, $\hat{\epsilon}_R = 347$. Z_I is attributed to the intermediate frequency resonance resulting in a lower

value for \mathcal{R} so that $R_I = 23 \Omega$. However, shifting the corresponding resonance frequency to the intermediate regime requires a significant correction of the interface capacity, i.e., $\zeta = 0.02$. Finally, $Z_{D,\text{SEI}}$ is parametrized so that its amplitude is small. In this case, $Z_{D,\text{SEI}}$ can be neglected if $\hat{t}_+ = 0.97$.

Both models show good qualitative agreement with the experiment, see fig. 8. Naturally, the first parametrization has a better quantitative agreement with the data as it correctly predicts the depressed semicircle. However, this depression could also be caused by an inhomogeneous distribution of SEI properties. The main parametrization also requires more reasonable corrections. For instance, the interface capacity needs to be corrected by a factor of 5 in the main whereas a factor of 50 is needed in the alternative one. Both parametrizations require large values for the relative permittivity of the SEI. However, the value needed in the alternative option is even larger so that it is difficult to justify (135 vs. 347). A better understanding of which parametrization is correct can be obtained by observing the high frequency impedance during the initial SEI formation. This would easily allow the identification of SEI impedance contributions which increase during this time.

Both parametrizations share a large lithium transference number to describe the transport in the SEI pores. Here, the values 0.9 and 0.97 are used, indicating that transport in the SEI pores is qualitatively different from transport in the bulk electrolyte. As argued above, this behavior can be explained by immobilization of anions in the porous SEI structure.⁵¹ Although these two values are similar, they cause a significant change in the cell impedance. In the first parametrization, $R_{D,\text{SEI}}$ is equal to 15Ω creating a visible resonance between the interface semicircle and the low frequency finite-length Warburg. In contrast, in the second parametrization, $R_{D,\text{SEI}}$ is equal to 1.5Ω so that $Z_{D,\text{SEI}}$ is overshadowed and not visible. Note that a smaller value of \hat{t}_+ would result in a much larger amplitude of $Z_{D,\text{SEI}}$ and can be ruled out. Therefore, the model predicts lithium-ion transference numbers close to one in the SEI phase.

In conclusion, the assumption that charge transfer in the SEI is facilitated by liquid electrolyte in small SEI pores predicts the emergence of an additional feature in the cell impedance. For the experiment at hand, this feature dominates the impedance response if the lithium-ion transference number in the SEI is not adjusted ($\hat{t}_+ = 0.0245 \rightarrow R_{D,\text{SEI}} = 1868 \Omega$). Our model only agrees with the experiment if large lithium-ion transference numbers are chosen in the SEI phase. This indicates that lithium ions move in the solid phase of the SEI or that lithium-ion transport in the SEI pores has solid-electrolyte character.

6 Conclusions

In this article, we present an analytical impedance model for a symmetric cell with planar electrodes. We model the solid-electrolyte interphase (SEI) as a porous surface layer. Our model relies on a thermodynamically consistent theory for electrolyte transport. We take special care that transport parameters as the diffusion coefficient and the transference numbers are well defined. This implies the consistent definition of a reference velocity, the center-of-mass velocity in our case. Our analytic expressions for impedance spectroscopy show that this is especially relevant for concentrated electrolytes.

To reveal the parameter dependence of the impedance spectrum, we perform a step-by-step procedure. We begin by calculating the impedance spectrum for locally electro-neutral systems without SEI. Finally, we relax the condition of local electro-neutrality and include transport through a porous SEI. Most importantly, we describe diffusion impedances or Warburg short elements and reveal their dependence on the transference number. Thus, we suggest to use impedance spectroscopy for the determination of the transference number or the thermodynamic factor in the bulk electrolyte and the SEI.

Our analytical impedance expressions are approximately described with common equivalent circuit models. We identify and discuss the frequency range and parameter space in which equivalent circuit methods are valid.

We predict the thickness of charged electrochemical double-layers based on the Poisson equation. Thus, in our model, the standard Debye length defines the double-layer capacitance and the resonance frequency of the interface reaction semicircle. However, this frequency does not agree with experimental data for a Li-TFSI tetraglyme solution with Li-metal electrodes. This indicates that charged double-layers of the reference state cannot be neglected when calculating the impedance response. Furthermore, ion adsorption on the electrode surface contributes significantly to the interface capacitance of this system.

Our model explores the assumption that charge transport through the SEI is enabled by small pores which are filled with electrolyte. This results in a second finite-length Warburg element in the impedance response of the cell. Only a SEI specific Li^+ transference number close to one reduces the amplitude of this impedance contribution to levels that align with experiments. Therefore, charge transport in the SEI shows the characteristics of a solid electrolyte even if transport in a liquid environment is assumed. We therefore propose to describe lithium-ion transport in the SEI with a specific theory for solid electrolytes.

Acknowledgement This work is supported by the German Federal Ministry of Education and Research (BMBF) with the project Li-EcoSafe (03X4636A). The authors thank Prof. Bernhard Roling and Fabian Sälzer for stimulating discussions.

References

- (1) Fauteux, D. Formation of a passivating film at the lithium-PEO-LiCF₃SO₃ interface. *Solid State Ionics* **1985**, *17*, 133–138, DOI: 10.1016/0167-2738(85)90061-X.
- (2) Gao, L.; Digby D, M. Characterization of Irreversible Processes at the Li/Poly[bis(2,3-di-(2-methoxyethoxy)propoxy)phosphazana] Interface on Charge Cycling. *Physics* **1988**, *21*, 4341–4345, DOI: 10.1093/isle/ist137.
- (3) Lu, P.; Li, C.; Schneider, E. W.; Harris, S. J. Chemistry, impedance, and morphology evolution in solid electrolyte interphase films during formation in lithium ion batteries. *Journal of Physical Chemistry C* **2014**, *118*, 896–903, DOI: 10.1021/jp4111019.
- (4) Steinhauer, M.; Risse, S.; Wagner, N.; Friedrich, K. A. Investigation of the Solid Electrolyte Interphase Formation at Graphite Anodes in Lithium-Ion Batteries with Electrochemical Impedance Spectroscopy. *Electrochimica Acta* **2017**, *228*, 652–658, DOI: 10.1016/j.electacta.2017.01.128.
- (5) Levi, M. D.; Aurbach, D. Simultaneous Measurements and Modeling of the Electrochemical Impedance and the Cyclic Voltammetric Characteristics of Graphite Electrodes Doped with Lithium. *The Journal of Physical Chemistry B* **1997**, *101*, 4630–4640, DOI: 10.1021/jp9701909.
- (6) Doyle, M. Modeling of Galvanostatic Charge and Discharge of the Lithium/Polymer/Insertion Cell. *Journal of The Electrochemical Society* **1993**, *140*, 1526, DOI: 10.1149/1.2221597.
- (7) Danner, T.; Singh, M.; Hein, S.; Kaiser, J.; Hahn, H.; Latz, A. Thick electrodes for Li-ion batteries: A model based analysis. *Journal of Power Sources* **2016**, *334*, 191–201, DOI: 10.1016/j.jpowsour.2016.09.143.
- (8) Fronczek, D. N.; Bessler, W. G. Insight into lithium-sulfur batteries: Elementary kinetic modeling and impedance simulation. *Journal of Power Sources* **2013**, *244*, 183–188, DOI: 10.1016/j.jpowsour.2013.02.018.
- (9) Danner, T.; Zhu, G.; Hofmann, A. F.; Latz, A. Modeling of nano-structured cathodes for improved lithium-sulfur batteries. *Electrochimica Acta* **2015**, *184*, 124–133, DOI: 10.1016/j.electacta.2015.09.143.
- (10) Schmitt, T.; Arlt, T.; Manke, I.; Latz, A.; Horstmann, B. Zinc electrode shape-change in secondary air batteries: A 2D modeling approach. *Journal of Power Sources* **2019**, *432*, 119–132, DOI: 10.1016/j.jpowsour.2019.126649.

- (11) Clark, S.; Mainar, A. R.; Iruin, E.; Colmenares, L. C.; Blázquez, J. A.; Tolchard, J. R.; Latz, A.; Horstmann, B. Towards rechargeable zinc-air batteries with aqueous chloride electrolytes. *J. Mater. Chem. A* **2019**, *7*, 11387–11399, DOI: 10.1039/C9TA01190K.
- (12) Clark, S.; Latz, A.; Horstmann, B. A Review of Model-Based Design Tools for Metal-Air Batteries. *Batteries* **2018**, *4*, 5, DOI: 10.3390/batteries4010005.
- (13) Jahnke, T.; Zago, M.; Casalegno, A.; Bessler, W. G.; Latz, A. A transient multi-scale model for direct methanol fuel cells. *Electrochimica Acta* **2017**, *232*, 215–225, DOI: 10.1016/j.electacta.2017.02.116.
- (14) Moya, A. A. Electrochemical Impedance of Ion-Exchange Membranes with Interfacial Charge Transfer Resistances. *Journal of Physical Chemistry C* **2016**, *120*, 6543–6552, DOI: 10.1021/acs.jpcc.5b12087.
- (15) Huang, Q. A.; Park, S. M. Unified model for transient faradaic impedance spectroscopy: Theory and prediction. *Journal of Physical Chemistry C* **2012**, *116*, 16939–16950, DOI: 10.1021/jp306140w.
- (16) Lück, J.; Latz, A. The electrochemical double layer and its impedance behavior in lithium-ion batteries. *Physical Chemistry Chemical Physics* **2019**, *21*, 14753–14765, DOI: 10.1039/C9CP01320B.
- (17) Braun, S.; Yada, C.; Latz, A. Thermodynamically Consistent Model for Space-Charge-Layer Formation in a Solid Electrolyte. *Journal of Physical Chemistry C* **2015**, *119*, 22281–22288, DOI: 10.1021/acs.jpcc.5b02679.
- (18) Hoffmann, V.; Pulletikurthi, G.; Carstens, T.; Lahiri, A.; Borodin, A.; Schammer, M.; Horstmann, B.; Latz, A.; Endres, F. Influence of a silver salt on the nanostructure of a Au(111)/ionic liquid interface: An atomic force microscopy study and theoretical concepts. *Physical Chemistry Chemical Physics* **2018**, *20*, 4760–4771, DOI: 10.1039/c7cp08243f.
- (19) Single, F.; Horstmann, B.; Latz, A. Dynamics and morphology of solid electrolyte interphase (SEI). *Phys. Chem. Chem. Phys.* **2016**, *18*, 17810–17814, DOI: 10.1039/C6CP02816K.
- (20) Horstmann, B.; Gallant, B.; Mitchell, R.; Bessler, W. G.; Shao-Horn, Y.; Bazant, M. Z. Rate-Dependent Morphology of Li₂O₂ Growth in Li-O₂ Batteries. *The Journal of Physical Chemistry Letters* **2013**, *4*, 4217–4222, DOI: 10.1021/jz401973c.
- (21) Legrand, N.; Raël, S.; Knosp, B.; Hinaje, M.; Desprez, P.; Lapticque, F. Including double-layer capacitance in lithium-ion battery mathematical models. *Journal of Power Sources* **2014**, *251*, 370–378, DOI: 10.1016/j.jpowsour.2013.11.044.
- (22) Bessler, W. G. Rapid Impedance Modeling via Potential Step and Current Relaxation Simulations. *Journal of The Electrochemical Society* **2007**, *154*, B1186, DOI: 10.1149/1.2772092.
- (23) Levi, M. D.; Aurbach, D. Impedance of a single intercalation particle and of non-homogeneous, multilayered porous composite electrodes for Li-ion batteries. *Journal of Physical Chemistry B* **2004**, *108*, 11693–11703, DOI: 10.1021/jp0486402.
- (24) Huang, R. W. J. M.; Chung, F.; Kelder, E. M. Impedance Simulation of a Li-Ion Battery with Porous Electrodes and Spherical Li⁺ Intercalation Particles. *Journal of The Electrochemical Society* **2006**, *153*, A1459, DOI: 10.1149/1.2203947.
- (25) Meyers, J. P.; Doyle, M.; Darling, R. M.; Newman, J. The Impedance Response of a Porous Electrode Composed of Intercalation Particles. *Journal of The Electrochemical Society* **2000**, *147*, 2930, DOI: 10.1149/1.1393627.
- (26) Song, J.; Bazant, M. Z. Effects of Nanoparticle Geometry and Size Distribution on Diffusion Impedance of Battery Electrodes. *Journal of the Electrochemical Society* **2012**, *160*, A15–A24, DOI: 10.1149/2.023301jes.
- (27) Schmidt, J. P.; Chrobak, T.; Ender, M.; Illig, J.; Klotz, D.; Ivers-Tiffée, E. Studies on LiFePO₄s cathode material using impedance spectroscopy. *Journal of Power Sources* **2011**, *196*, 5342–5348, DOI: 10.1016/j.jpowsour.2010.07.071.
- (28) Murbach, M. D.; Schwartz, D. T. Extending Newman's Pseudo-Two-Dimensional Lithium-Ion Battery Impedance Simulation Approach to Include the Nonlinear Harmonic Response. *Journal of The Electrochemical Society* **2017**, *164*, E3311–E3320, DOI: 10.1149/2.030171jes.
- (29) Kulikovskiy, A. A physical model for catalyst layer impedance. *Journal of Electroanalytical Chemistry* **2012**, *669*, 28–34, DOI: 10.1016/j.jelechem.2012.01.018.
- (30) Kulikovskiy, A.; Eikerling, M. Analytical solutions for impedance of the cathode catalyst layer in PEM fuel cell : Layer parameters from impedance spectrum without fitting. *Journal of Electroanalytical Chemistry* **2013**, *691*, 13–17, DOI: 10.1016/j.jelechem.2012.12.002.
- (31) Kulikovskiy, A.; Shamardina, O. A Model for PEM Fuel Cell Impedance : Oxygen Flow in the Channel Triggers Spatial and Frequency Oscillations.

- Journal of The Electrochemical Society* **2015**, *162*, 1068–1077, DOI: 10.1149/2.0911509jes.
- (32) Zhou, H.; Preston, M. A.; Tilton, R. D.; White, L. R. Calculation of the dynamic impedance of the double layer on a planar electrode by the theory of electrokinetics. *Journal of Colloid and Interface Science* **2005**, *292*, 277–289, DOI: 10.1016/j.jcis.2005.05.037.
- (33) Wohde, F.; Balabajew, M.; Roling, B. Li Transference Numbers in Liquid Electrolytes Obtained by Very-Low-Frequency Impedance Spectroscopy at Variable Electrode Distances. *Journal of The Electrochemical Society* **2016**, *163*, A714–A721, DOI: 10.1149/2.0811605jes.
- (34) Schammer, M.; Latz, A.; Horstmann, B. Transport Theory of Strongly Correlated Electrolytes. *In Submission* **2019**,
- (35) Latz, A.; Zausch, J. Multiscale modeling of lithium ion batteries: Thermal aspects. *Beilstein Journal of Nanotechnology* **2015**, *6*, 987–1007, DOI: 10.3762/bjnano.6.102.
- (36) Latz, A.; Zausch, J. Thermodynamic Consistent Transport Theory of Li-ion Batteries. *Journal of Power Sources* **2011**, *196*, 3296–3302, DOI: 10.1016/j.jpowsour.2010.11.088.
- (37) Stamm, J.; Varzi, A.; Latz, A.; Horstmann, B. Modeling nucleation and growth of zinc oxide during discharge of primary zinc-air batteries. *Journal of Power Sources* **2017**, *360*, 136–149, DOI: 10.1016/j.jpowsour.2017.05.073.
- (38) Clark, S.; Latz, A.; Horstmann, B. Rational Development of Neutral Aqueous Electrolytes for Zinc-Air Batteries. *ChemSusChem* **2017**, *10*, 4735–4747, DOI: 10.1002/cssc.201701468.
- (39) Horstmann, B.; Danner, T.; Bessler, W. G. Precipitation in aqueous lithium-oxygen batteries: A model-based analysis. *Energy and Environmental Science* **2013**, *6*, 1299–1314, DOI: 10.1039/c3ee24299d.
- (40) Rubi, J. M.; Kjelstrup, S. Mesoscopic Nonequilibrium Thermodynamics Gives the Same Thermodynamic Basis to Butler-Volmer and Nernst Equations. *The Journal of Physical Chemistry B* **2003**, *107*, 13471–13477, DOI: 10.1021/jp030572g.
- (41) Latz, A.; Zausch, J. Thermodynamic derivation of a Butler-Volmer model for intercalation in Li-ion batteries. *Electrochimica Acta* **2013**, *110*, 358–362, DOI: 10.1016/j.electacta.2013.06.043.
- (42) Bazant, M. Z. Theory of Chemical Kinetics and Charge Transfer based on Nonequilibrium Thermodynamics. *Accounts of Chemical Research* **2013**, *46*, 1144–1160, DOI: 10.1021/ar300145c.
- (43) Harris, S. J.; Lu, P. Effects of inhomogeneities - Nanoscale to mesoscale - on the durability of Li-ion batteries. *Journal of Physical Chemistry C* **2013**, *117*, 6481–6492, DOI: 10.1021/jp311431z.
- (44) Michan, A. L.; Leskes, M.; Grey, C. P. Voltage Dependent Solid Electrolyte Interphase Formation in Silicon Electrodes: Monitoring the Formation of Organic Decomposition Products. *Chemistry of Materials* **2015**, 385–398, DOI: 10.1021/acs.chemmater.5b04408.
- (45) Single, F.; Horstmann, B.; Latz, A. Revealing SEI Morphology: In-Depth Analysis of a Modeling Approach. *Journal of The Electrochemical Society* **2017**, *164*, E3132–E3145, DOI: 10.1149/2.0121711jes.
- (46) Single, F.; Latz, A.; Horstmann, B. Identifying the Mechanism of Continued Growth of the Solid-Electrolyte Interphase. *ChemSusChem* **2018**, *11*, 1950–1955, DOI: 10.1002/cssc.201800077.
- (47) Horstmann, B.; Single, F.; Latz, A. Review on multi-scale models of solid-electrolyte interphase formation. *Current Opinion in Electrochemistry* **13**, 61–69, DOI: 10.1016/j.coelec.2018.10.013.
- (48) Newman, J. S.; Tobias, C. W. Theoretical Analysis of Current Distribution in Porous Electrodes. *Journal of The Electrochemical Society* **1962**, *109*, 1183, DOI: 10.1149/1.2425269.
- (49) Newman, J.; Tiedemann, W. Porous-electrode theory with battery applications. *AIChE Journal* **1975**, *21*, 25–41, DOI: 10.1002/aic.690210103.
- (50) Newman, J.; Thomas-Alyea, K. E. *Electrochemical Systems*; John Wiley & Sons, 2004.
- (51) Popovic, J.; Hasegawa, G.; Moudrakovski, I.; Maier, J. Infiltrated porous oxide monoliths as high lithium transference number electrolytes. *Journal of Materials Chemistry A* **2016**, *4*, 7135–7140, DOI: 10.1039/c6ta01826b.
- (52) Warburg, E. Ueber die Polarisationscapacität des Platins. *Annalen der Physik* **1901**, *311*, 125–135, DOI: <https://doi.org/10.1002/andp.19013110910>.
- (53) Neumann, E. Ueber die Polarisationscapacität umkehrbarer Elektroden. *Annalen der Physik* **1899**, *303*, 500–534, DOI: 10.1002/andp.18993030303.
- (54) Payne, R.; Theodorou, I. E. Dielectric properties and relaxation in ethylene carbonate and propylene carbonate. *Journal of Physical Chemistry* **1972**, *76*, 2892–2900, DOI: 10.1021/j100664a019.
- (55) Biesheuvel, P. M.; Fu, Y.; Bazant, M. Z. Diffuse charge and Faradaic reactions in porous electrodes. *Phys. Rev. E* **2011**, *83*, 061507, DOI: 10.1103/PhysRevE.83.061507.

- (56) Lück, J.; Latz, A. Theory of reactions at electrified interfaces. *Physical Chemistry Chemical Physics* **2016**, *18*, 17799–17804, DOI: 10.1039/c6cp02681h.
- (57) Peled, E. The Electrochemical Behavior of Alkali and Alkaline Earth Metals in Nonaqueous Battery Systems – The Solid Electrolyte Interphase Model. *Journal of The Electrochemical Society* **1979**, *126*, 2047–2051, DOI: 10.1149/1.2128859.
- (58) Broussely, M.; Herreyre, S.; Biensan, P.; Kasztejna, P.; Nechev, K.; Staniewicz, R. J. Aging Mechanism in Li Ion Cells and Calendar Life Predictions. *Journal of Power Sources* **2001**, *97-98*, 13–21, DOI: 10.1016/S0378-7753(01)00722-4.
- (59) Brouillette, D.; Perron, G.; Desnoyers, J. E. Apparent Molar Volume, Heat Capacity, and Conductance of Lithium Bis (trifluoromethylsulfone) imide in Glymes and Other Aprotic Solvents. *Journal of Solution Chemistry* **1998**, *27*, 151–182, DOI: 10.1023/A:1022609407560.
- (60) Dong, D.; Sälzer, F.; Roling, B.; Bedrov, D. How efficient is Li⁺ ion transport in solvate ionic liquids under anion-blocking conditions in a battery? *Physical Chemistry Chemical Physics* **2018**, *20*, 29174–29183, DOI: 10.1039/C8CP06214E.
- (61) Doyle, M. Analysis of Transference Number Measurements Based on the Potentiostatic Polarization of Solid Polymer Electrolytes. *Journal of The Electrochemical Society* **1995**, *142*, 3465, DOI: 10.1149/1.2050005.
- (62) Ehrl, A.; Graf, M.; Wall, W. A.; Gasteiger, H. A.; Landesfeind, J. Direct Electrochemical Determination of Thermodynamic Factors in Aprotic Binary Electrolytes. *Journal of The Electrochemical Society* **2016**, *163*, A1254–A1264, DOI: 10.1149/2.0651607jes.
- (63) Naejus, R.; Lemordant, D. Excess thermodynamic properties of binary mixtures containing linear or cyclic carbonates as solvents at the temperatures 298.15 K and 315.15 K. *The Journal of Chemical Thermodynamics* **1997**, *29*, 1503–1515, DOI: 10.1006/jcht.1997.0260.